ORIGINAL ARTICLE

Neuropathological examination of fetal rat brain in the 5-bromo-2′-deoxyuridine-induced neurodevelopmental disorder model

Tetsuo Ogawa, Makiko Kuwagata, Katsumasa T. Muneoka, and Seiji Shioda
Department of Anatomy, Showa University School of Medicine, Tokyo, Japan

ABSTRACT **The majority of prior developmental neurotoxicity studies focused on postnatal subjects rather than on the fetus. In the present paper, we demonstrate the use of histological examination of fetal rat (embryonic day 16.5) brain serial sections, employing Nissl staining and microtubule-associated protein 2 (MAP2) immunohistochemistry, in evaluating a chemical-induced neurodevelopmental disorder. Since prenatal treatment with 5-bromo-2′-deoxyuridine (BrdU) is known to induce behavioral abnormalities such as locomotor hyperactivity in offspring, pregnant rats were administered 50 mg/kg on gestation days 9.5 through 15.5. The fetal brains at embryonic day 16.5 were collected and processed for neuropathological study. Cell death, including DNA strand breaks, was observed in specific areas of the fetal brain such as the neuroepithelium, intermediate zone and/or differentiating zones (e.g. neocortex and striatum) in exposed fetuses. In addition, the neocortex had an abnormal appearance cortical plate, which was also detected by MAP2 immunohistochemistry. The abnormal cortical plate was observed consistently, while the grade of cell death was generally very mild and variable. No significant alteration was detected in the brainstem. The present study reveals that histological observation of the fetal brain includes sensitive endpoints in developmental neurotoxicity, and that BrdU, at a dose generally administered to label proliferating cells, affects the development of the fetal neocortex.**

Key Words: BrdU, developmental neurotoxicity, neurodevelopmental disorder, neuropathology

INTRODUCTION

Prenatal exposure to chemicals such as alcohol, polychlorinated biphenyls (PCBs) and valproic acid are known to induce developmental abnormalities in the central nervous system of children (Jacobson & Jacobson 1996; Rogan *et al.* 1988; Moore *et al.* 2000; Williams *et al.* 2001; Burd *et al.* 2003). In developmental neurotoxicity, the majority of studies focus on the postnatal subjects rather than on the fetus. Even in the study of endocrine disrupters, an area of current scientific interest, there has been little focus on the assessment of alterations in the fetal brain shortly after experimental *in utero* chemical exposure. Among the reasons for this are (i) the difficulty in obtaining histological preparations of satisfactory quality and level of section; and (ii) the absence of clear endpoints for use in histological evaluation of such material. Despite such difficulties, the evaluation of the fetal brain is an important step in assessing toxic alterations during neurodevelopment. Accumulation of findings from the fetal brain after prenatal chemical exposure is important. In the present paper, we demonstrate our method of preparing serial sections containing a wide variety of fetal brain areas, and the use of microtubule-associated protein 2 (MAP2) immunohistochemistry to demonstrate *in utero* neuropathological changes in an experimental neurodevelopmental disorder model (Kuwagata *et al.* 2004).

5-Bromo-2′-deoxyuridine (BrdU), a thymidine analog, is incorporated into the DNA as 5-bromouracil during the synthesis phase of the cell cycle (Schwartz & Kirsten 1974; Yu 1976; 1977; Biggers *et al.* 1987), and has been used extensively as a useful tool for labeling proliferating cells in cancer research and developmental neuroscience (Miller & Nowakowski 1988; Soriano & Del Rio 1991; Takahashi *et al.* 1999). However, several lines of evidence have revealed that BrdU has genotoxicity (Morris 1991). Interestingly, prenatal exposure to BrdU, even at a dose generally administered to adult rodents (50 mg/kg), is reported to induce behavioral abnormalities, such as locomotor hyperactivity, and the possibility of the exposed offspring as an animal model of developmental brain disorders, such as attention-deficit hyperactivity disorder (ADHD) has been discussed (Nagao *et al.* 1997; Kuwagata & Nagao 1998; Kuwagata *et al.* 2001; 2004). In the study presented here we evaluated structural changes induced in the fetal rat brain shortly after BrdU exposure.

MATERIALS AND METHODS

Animals and BrdU treatment

Sprague–Dawley rats (7–9 weeks of age) were purchased from Japan SLC Co. (Hamamatsu, Japan). The animals were housed at the Animal Institution at Showa University. They were kept in cages in a ventilated animal room with controlled temperature and relative humidity, with a 12 h light : 12 h dark schedule (lights on at 06:00 hours) with access to food and tap water *ad libitum*. All animal experiments were started after an acclimation period of at least 1 week. Pregnant animals were obtained by housing females with males (one to two females per male). The day when sperm in vaginal smears was observed in the morning was designated as gestation day 0.5 (GD 0.5) and embryonic day 0.5.

BrdU (Sigma, St Louis, MO, USA) was suspended in 0.5% sodium carboxymethyl cellulose (CMC Na) and administered immediately. This compound was administered intraperitoneally to five pregnant rats on GD 9.5 through 15.5 at a defined time (12:00–13:00 hours), at a dose of 50 mg/kg. Four control dams received 0.5% CMC Na (5 mL/kg) on GD 9.5 through 15.5. The dosages were based on the body weight on GD 9.5.

Correspondence: Tetsuo Ogawa, PhD, Showa University School of Medicine, Department of Anatomy, 1-5-8 Hatanodai Shinagawa-ku, Tokyo 142-8555, Japan. Email: t.ogawa@med.showa-u.ac.jp

Received September 6, 2004; revised and accepted October 22, 2004.

Preparation of fetal rat brains for neuropathological examination

On GD 16.5 (24 h after the final treatment with BrdU) the rats were deeply anesthetized by pentobarbital (50 mg/kg, i.p.) and the gravid uterus was removed and placed in 10 mM phosphate buffer, pH 7.4, containing saline (PBS) on ice. Fetuses were removed and their brains were excised carefully, but quickly. The brains were placed in 4% paraformaldehyde in 0.1 M phosphate buffer, pH 7.4 and stored at 4°C for 2 days. Following this, the specimens were embedded in 10% gelatin and coronal sections were cut at a thickness of 45 μm in a vibratome. All of the serial sections were collected and maintained in PBS supplemented with 0.05% sodium azide. Every third section was incubated overnight in a solution of PBS containing 5% normal goat serum and 0.3% Triton X-100, mounted on slide glass and processed for Nissl staining. Eighteen fetuses in each group (from four dams in the control and five dams in the BrdU group) were studied histopathologically. The grading methods and results of these pathological observations are described in Table 1.

Another series of every third section (four fetuses from two dams in each group) was subjected to MAP2 immunohistochemical staining. The sections were incubated in a free-floating manner at each of the following steps. After inactivation of endogenous peroxidase in 10 mM PBS containing 3% H_2O_2 for 15 min and washing in 10 mM PBS (5 min × three washes), the sections were transferred to a blocking solution (PBS containing 5% normal goat serum and

Table 1 Neuropathological findings in the fetal rat brain (embryonic day 16.5) treated with BrdU at age E9.5–15.5

		Control ($n = 18$)					BrdU ($n = 18$)				
Area	Finding	±	+	++	+++	Total	±	+	++	+++	Total
Frontal neocortex	Cell death in N and IZ	5	0	0	0	5	0	14	2	2	18**
	CD					0					17**
Septum	Cell death	4	0	0	0	4	6	0	0	0	6
Basal telencephalic N	Cell death	0	0	0	0	0	0	2	0	0	2
Striatum	Cell death in D	0	0	0	0	0	8	4	2	0	14**
Amygdala	Cell death	0	0	0	0	0	0	0	0	0	0
Thalamus, anterior	Cell death	0	0	0	0	0	5	1	1	0	7***
Hypothalamus											
Preoptic area, medial	Cell death in D	0	0	0	0	0	6	3	0	0	9***
Preoptic area, lateral	Cell death in D	0	0	0	0	0	4	0	0	0	4**
Anterior	Cell death in N and D	2	0	0	0	2	5	1	0	0	6
Lateral	Cell death	4	0	0	0	4	1	1	0	0	2
Ventro-dorsal medial	Cell death	3	0	0	0	3	3	2	0	0	5
Posterior	Cell death	0	0	0	0	0	3	3	0	0	6***
Mammillary body	Cell death	2	0	0	0	2	6	5	0	0	11**
Central neocortex	Cell death in N and IZ	4	0	0	0	4	3	12	1	1	17**
	CD					0					16**
Hippocampus	Cell death in N	5	0	0	0	5	2	12	3	0	17**
	Cell death in D	3	0	0	0	3	6	9	2	0	17**
Posterior neocortex	Cell death in N and IZ	1	0	0	0	1	4	9	1	1	15**
Substantia nigra, ventral segmental area (A9, 10)	Cell death	0	0	0	0	0	0	0	0	0	0
Central gray	Cell death	11	4	0	0	15	17	1	0	0	18
Superior colliculus	Cell death	4	0	0	0	4	8	2	2	0	12**
Inferior colliculus	Cell death	9	0	0	0	9	9	4	2	0	15*
Raphe		0	0	0	0	0	0	0	0	0	0
Medulla oblongata, facial motor nucleus	Cell death	0	0	0	0	0	0	0	0	0	0
Cerebellum	Cell death	10	2	0	0	12	16	2	0	0	18**

CD, cortical dysgenesis (lower cellularity and disrupted arrangement of precursor cells in the cortical plate) in neocortex and insular cortex; D, differentiating field; IZ, intermediate zone; N, neuroepithelium. –, no finding; ±, observed with very low frequency; +, observed at least one on each field observed at × 400 magnification or on each section; ++, observed a few on each field observed at × 400 magnification; +++, observed several on each field observed at × 400 magnification. *$P < 0.05$; **$P < 0.01$ compared with the control group by χ^2 test; ***$P < 0.01$ compared with the control group by Fisher's exact test.

0.3% Triton X-100) and incubated for 1 h. The sections were then incubated in a blocking solution containing the primary antibody (monoclonal mouse anti-MAP2a + 2b [Sigma, St Louis, MO, USA] used at a 1 : 500 dilution) at 4°C for 2 days. The primary antibody was washed out in 10 mM PBS (5 min × 3 washes) and the sections were then incubated with the secondary antibody (biotinylated anti-mouse IgG; Vector laboratories, Burlingame, CA, USA) diluted in the blocking solution (1 : 200) for 90 min. After washing out the secondary antibody, the sections were subjected to an avidin/biotin-immunoperoxidase reaction using a Vectastain ABC kit (Vector laboratories) with visualization of the antigen using diaminobenzidine as a substrate. Lastly, sections from three fetuses, which included the anterior neocortex, were selected from each group and processed for TUNEL staining by an In Situ Cell Death Detection Kit, POD (Roche Molecular Biochemicals, Mannheim, Germany).

All animal care and experimental procedures were approved by the Institutional Animal Care and Use Committee of Showa University.

The incidence of pathological findings was analyzed statistically using Fisher's exact test when the lowest expected number was less than 5, or χ^2 test when the lowest expected number was 5 or greater than 5. A *P*-value less than 0.05 was considered statistically significant.

RESULTS

The fetal brain areas observed are presented in Fig. 1. The method described here consistently made it possible to observe a wide variety of fetal brain areas, from the frontal neocortex to the cerebellum and medulla oblongata. In the controls, cell death was occasionally observed in the neuroepithelia of several brain areas and the intermediate zone of the neocortex, and in some neuroepithelial and differentiating zones, including the hippocampus, midbrain and cerebellum (Table 1). In the intermediate zone of the neocortex, a few proliferating cells were also observed.

The findings in the neuropathological observation of the fetuses are shown in Table 1. Prenatal exposure to BrdU induced cell death in the neuroepithelium of the neocortex, hippocampus, striatum and the intermediate zone of the neocortex (Fig. 2). TUNEL staining revealed that the cell death included DNA strand breaks (Fig. 3). BrdU also induced cortical dysgenesis (lower cellularity and disrupted arrangement of immature neurons in the cortical plate) in the neocortex (Fig. 4). Abnormal cortical plates were observed consistently while the grade of cell death was in general very mild and variable, even in the same litter. In contrast to the findings in the forebrain, no significant change was observed in the brainstem areas, although two fetuses were very sensitive to BrdU and had some abnormalities in the midbrain (Table 1).

MAP2 immunohistochemistry using serial sections clearly demonstrated the distribution of immunoreactivity. MAP2 immunoreactivity was observed in several areas of the differentiating zones. MAP2 immunoreactivity was detected in the subplate and layer 1 of the neocortex with greater reactivity at the ventral-lateral areas, but less at the dorsal areas (Fig. 5a,c). MAP2 immunoreactivities were detected even in the altered cortical plates. However, the staining pattern reflected the pathologic findings (lower cellularity and disrupted arrangement of immature neurons) (Fig. 5b,d). In general, brainstem areas, which are known to start and terminate proliferation earlier, showed relatively greater MAP-2 immunoreactivity. There were no differences in MAP2 immunoreactivity between the control and BrdU exposures in the brainstem areas (data not shown).

DISCUSSION

As described in Introduction, the majority of studies on the developmental neurotoxicity focused on the postnatal subjects rather than the fetus, with behavioral endpoints being very common in the risk assessment evaluations. However, these endpoints, such as open-field behavior, are well known to be affected by prenatal and/or postnatal environmental factors (Ogawa *et al.* 1994; Lehmann *et al.* 2000; Hsu *et al.* 2003), suggesting that the results may include false-positives, or findings which are difficult to reproduce in other laboratories. Direct observation of effects in the fetal brain shortly after toxicant exposure is, in our opinion, one of the most reliable approaches to confirm subsequent postnatal changes in behavior or other endpoints. The method for preparation and sectioning of the fetal brain described in the present study is considered useful for this purpose. We used serial sectioning, Nissl staining and MAP2 immunohistochemistry, which made it possible to observe changes in a wide variety of brain areas. Although some studies have focused on the fetal brain, they described only specific areas such as the neocortex and hypothalamus, while few studies observed a wide variety of brain areas as in this study (Webster *et al.* 1973; Nagao *et al.* 1998; Fujimori *et al.* 2002; Yamauchi *et al.* 2004).

Neuropathologists may claim that vibratome sections at a thickness of 45 μm are good for immunohistochemistry, but they are too thick for neuropathological evaluation and significant information will be missed. However, our sections were good enough to demonstrate that BrdU, even at a dose generally used, induces cell death and abnormal cortical plate formation in the fetal brain.

BrdU is a compound which has been extensively used as a tool for labeling proliferating cells in cancer research and developmental neuroscience, including stem cell studies (Miller & Nowakowski 1988; Soriano & Del Rio 1991; Takahashi *et al.* 1999; Lindvall & McKay 2003). Doses ranging from 10 to 100 mg/kg are commonly injected into animals, and the dose of 50 mg/kg used in the present study is considered not to have significant general toxicity. Several lines of evidence have revealed that BrdU has genotoxicity (review: Morris 1991). It has been reported that BrdU shows two types of mutagenesis in mammalian cells (i) incorporation mutagenesis which occurs when BrdU triphosphate is incorporated into DNA; and (ii) replication mutagenesis which occurs when the BrdU-containing DNA replicates (Morris 1991). Furthermore, prenatal treatment with BrdU ranging from 400 to 1000 mg/kg results in a variety of fetal malformations, including those of the palate and face (Murphy 1965; Skalko *et al.* 1971) and the neural tube (Ruffolo & Ferm 1965; Webster *et al.* 1973). Webster *et al.* (1973) observed induction of prominent cell death in the neuroepithelium, intermediate zone and cortical plate 24 h after a single injection of 400–600 mg/kg of BrdU, which is very similar to findings in two fetuses in the present study (Table 1). Prenatal exposure to BrdU, even at a dose generally administered to adult rodents (50 mg/kg), is reported to induce behavioral abnormalities such as altered sexual behavior, impaired learning and memory, and locomotor hyperactivity (Nagao *et al.* 1997; Kuwagata & Nagao 1998; Kuwagata *et al.* 2001; 2004). The present study clearly revealed that this dosage of BrdU induces cell death in specific areas of fetal brain such as the neuroepithelium, intermediate zone and/or differentiating zones in, e.g. the neocortex and striatum. This suggests that the fetal brain, an actively proliferating tissue, is highly susceptible to genotoxic chemicals such as BrdU.

In addition to cell death, abnormal cortical plate appearance was induced shortly after BrdU exposure. The cell death observed in the intermediate zone may disturb the radial and tangential migrations of normal neuronal progenitor cells, which are known to

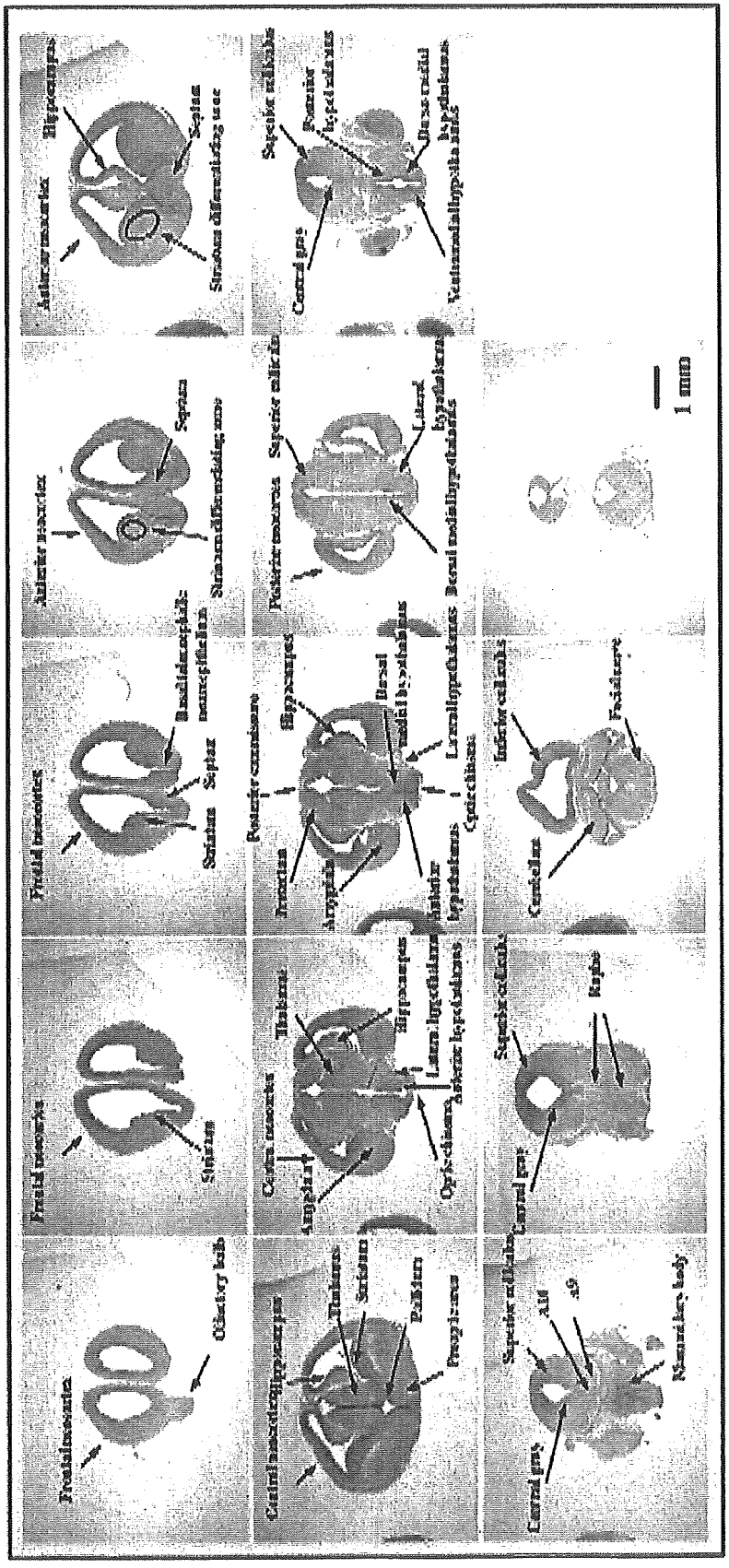

Fig. 1 Serial sections of a fetal rat brain at embryonic day 16.5. Nissl staining. The method for preparation and sectioning of the fetal brain described in the present study makes it possible to observe a wide variety of fetal brain areas.

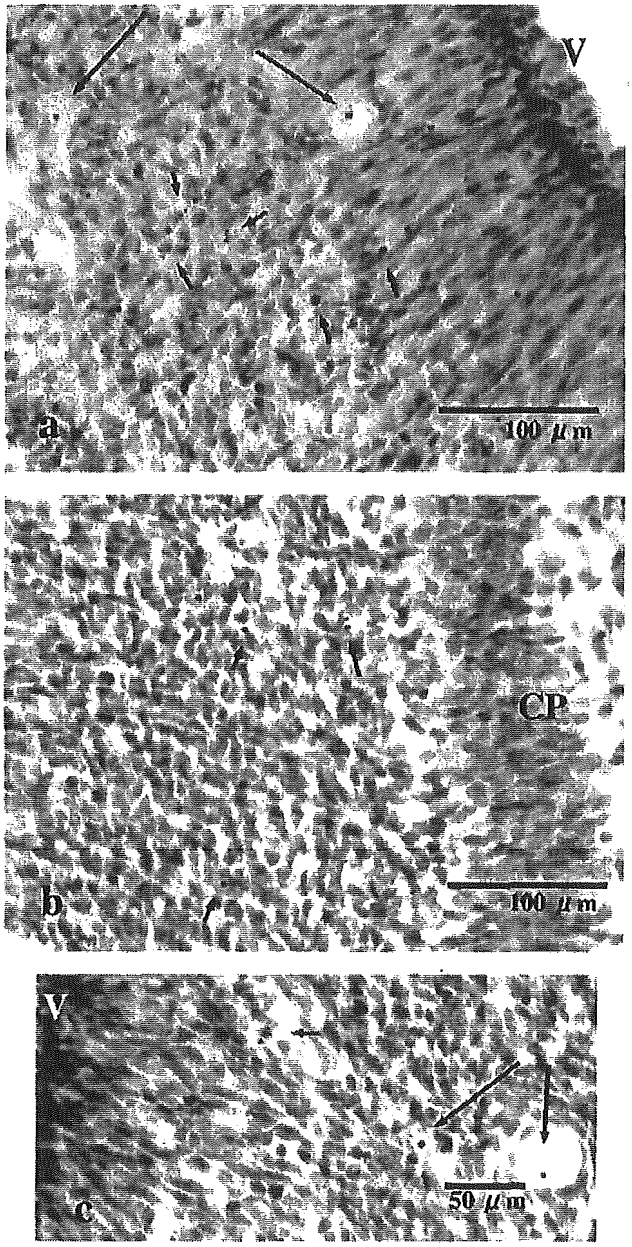

Fig. 2 Fetal rat brains (embryonic day 16.5) 24 h after the final treatment with BrdU. **A**: Cell death in the intermediate zone and neuroepithelium, grade +++. **B**: Cell death in the intermediate zone, grade ++. **C**: Cell death in the neuroepithelium, grade +. The short arrows indicate dead cells with pyknotic nuclei. The long arrows indicate monocytes. CP, cortical plate; V, ventricle.

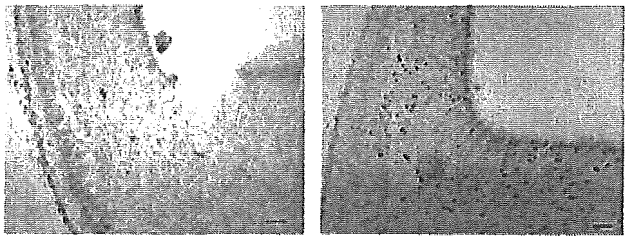

Fig. 3 TUNEL staining of fetal rat brains (embryonic day 16.5) 24 h after the final treatment with BrdU. Sections including the anterior neocortex and striatum were processed for TUNEL staining. Much TUNEL positive reactivity was observed in the brains treated with BrdU. The results indicate that BrdU induces cell death, including DNA strand breaks. Bars, 100 μm.

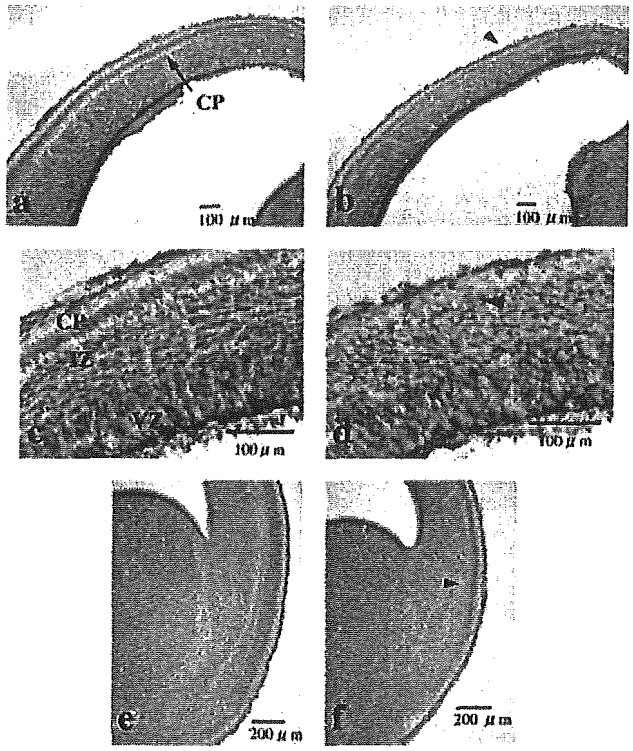

Fig. 4 Fetal rat brains (embryonic day 16.5) 24 h after the final treatment with BrdU. **A**: Neocortex of a control fetus. **B**: Neocortex of a fetus treated with BrdU. BrdU induced cortical dysgenesis (lower cellularity and disrupted arrangement of precursor cells in the cortical plate) in the neocortex. The arrowheads indicate an abnormal cortical plate. **C**: Neocortex of the control fetus (higher magnification); **D**: Neocortex of a fetus treated with BrdU (higher magnification). Disrupted arrangement of precursor cells in the cortical plate is observed (arrow head). **E**: Insular cortex of a control fetus. **F**: Insular cortex of a fetus treated with BrdU. BrdU induced cortical dysgenesis (lower cellularity) in the insular cortex. CP, cortical plate; IZ, intermediate zone; VZ, ventricular zone.

differentiate to glutamate and GABA neurons in the adult cerebral cortex (Tamamaki *et al.* 1997; Anderson *et al.* 2001; Marin & Rubenstein 2003). The abnormality in the cortical plate is probably produced by both the cell death in the neuroepithalia and intermediate zone, and the resulting disturbance to normal cell migration. This cortical plate abnormality was observed most consistently among the BrdU-exposed fetuses, although there was a variation in the degree of cell death, even in the same litter. Thus, observation of cortical plate is considered to be a sensitive endpoint.

MAP2 is the most prominent microtubule-associated protein of the neuronal cytoskeleton, and exists as a pair of high-molecular

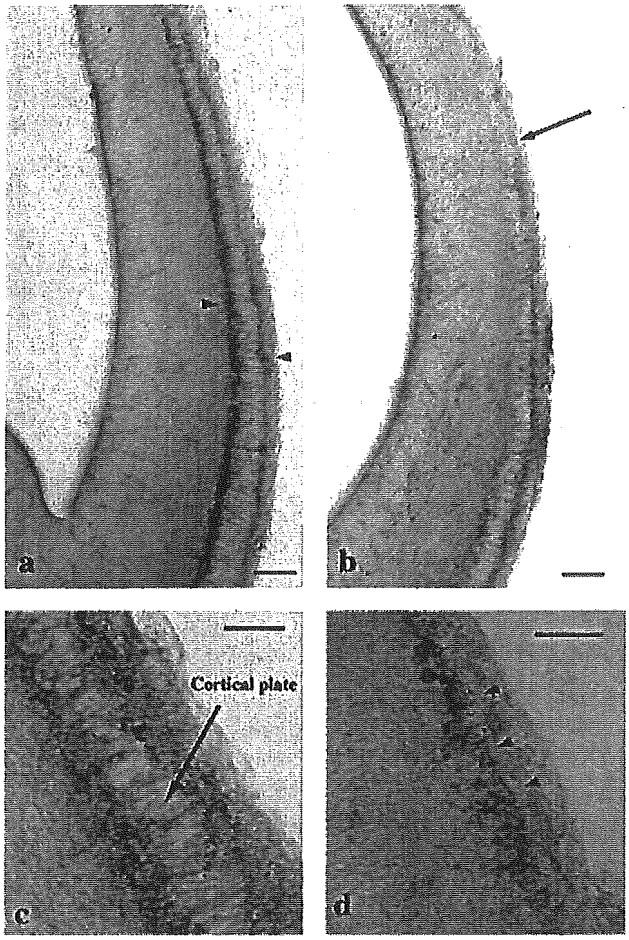

Fig. 5 MAP2 immunoreactivities of the fetal rat brain (embryonic day 16.5) 24 h after the final treatment with BrdU. **A:** MAP2 immunoreactivity is observed in the subplate and layer 1 of the neocortex (arrow heads) in the control brain. **B:** MAP2 immunoreactivity is very weak in the brain treated with BrdU (arrow). **C:** Higher magnification of another control brain. MAP2 immunoreactivity is observed in the subplate and layer 1 of the neocortex. **D:** Higher magnification of another brain treated with BrdU. Although cells in the cortical plate of the brain treated with BrdU expressed the MAP2 immunoreactivity (arrowheads), the staining pattern reflected the pathologic findings (lower cellularity and disrupted arrangement of immature neurons). Bars, 100 μm.

weight (280 kDa) forms, MAP2a and MAP2b, and a smaller form (70 kDa), MAP2c. MAP2c is particularly abundant in the developing brain (Fujimori *et al.* 2002). The high-molecular weight form is expressed in dendrites, and is often used as a neuronal marker *in vitro*, especially in stem cell studies (Izant & McIntosh 1980; Greene *et al.* 1983; Ferreira *et al.* 1987; Erlandsson *et al.* 2001). Thus, we decided to observe the high-molecular weight MAP2 immunoreactivity to examine the effect of prenatal chemical exposure on neural differentiation and maturation. In BrdU-induced developmental neurotoxicity, results from MAP2 immunohistochemistry supported the findings detected by Nissl staining sections. MAP2 immunoreactivity was still observed in the cortical plate after BrdU exposure, suggesting BrdU affects cell proliferation and migration, but not differentiation or maturation. Further studies to discriminate cell populations such as glutamate and GABA neurons may provide additional information on abnormalities in the neocortex, and help to explain the behavioral abnormalities in BrdU-exposed rats. MAP2 immunohistochemistry was also of use to show normally developing (differentiating) brain areas and the specificity of the BrdU toxicity in this study.

Since no significant alteration was observed in the midbrain and pons, a disrupted balance of development among brain areas (e.g. neocortex vs. brainstem; monoaminergic fibers are extending normally, but immature neural cells are not ready to accept them) may contribute to behavioral abnormalities in the offspring.

The use of study methods for the fetal brain described in the present report will help in the collection of *in utero* neuropathological findings in other neurodevelopmental disorders. Such data will contribute to an understanding of the causes of developmental brain disorders and will also lead to an improvement in current risk assessment.

ACKNOWLEDGMENTS

The authors thank Dr Bernard S. Jortner in Virginia Tech for reading this manuscript and providing comments.

REFERENCES

Anderson SA, Marin O, Horn C, Jennings K, Rubenstein JL (2001) Distinct cortical migrations from the medial and lateral ganglionic eminences. *Development* **128**: 353–363.

Biggers WJ, Barnea ER, Sanyal MK (1987) Anomalous neural differentiation induced by 5-bromo-2′-deoxyuridine during organogenesis in the rat. *Teratology* **35**: 63–75.

Burd L, Klug MG, Martsolf JT, Kerbeshian J (2003) Fetal alcohol syndrome: Neuropsychiatric phenomics. *Neurotoxicol Teratol* **25**: 697–705.

Erlandsson A, Enarsson M, Forsberg-Nilsson K (2001) Immature neurons from CNS stem cells proliferate in response to platelet-derived growth factor. *J Neurosci* **21**: 3483–3491.

Ferreira A, Busciglio J, Caceres A (1987) An immunocytochemical analysis of the ontogeny of the microtubule-associated proteins MAP-2 and Tau in the nervous system of the rat. *Brain Res Dev Brain Res* **431**: 9–31.

Fujimori K, Takauji R, Tamamaki N (2002) Differential localization of high- and low-molecular-weight variants of microtubule-associated protein 2 in the developing rat telencephalon. *J Comp Neurol* **449**: 330–342.

Greene LA, Liem RK, Shelanski ML (1983) Regulation of a high molecular weight microtubule-associated protein in PC12 cells by nerve growth factor. *J Cell Biol* **96**: 76–83.

Hsu FC, Zhang GJ, Raol YS, Valentino RJ, Coulter DA, Brooks-Kayal AR (2003) Repeated neonatal handling with maternal separation permanently alters hippocampal GABAA receptors and behavioral stress responses. *Proc Natl Acad Sci USA* **100**: 12213–12218.

Izant JG, McIntosh JR (1980) Microtubule-associated proteins: A monoclonal antibody to MAP2 binds to differentiated neurons. *Proc Natl Acad Sci USA* **77**: 4741–4745.

Jacobson JL, Jacobson SW (1996) Intellectual impairment in children exposed to polychlorinated biphenyls in utero. *N Engl J Med* **335**: 783–789.

Kuwagata M, Nagao T (1998) Behavior and reproductive function of rat male offspring treated prenatally with 5-bromo-2′-deoxyuridine. *Reprod Toxicol* **12**: 541–549.

Kuwagata M, Saito Y, Usumi K, Ono H, Nagao T (2001) Disruption of brain development in male rats exposed prenatally to 5-bromo-2′-deoxyuridine. *Cong Anom* **41**: 312–320.

Kuwagata M, Muneoka KT, Ogawa T, Takigawa M, Nagao T (2004) Locomotor hyperactivity following prenatal exposure to 5-bromo-2′-deoxyuridine: Neurochemical and behavioral evidence of dopaminergic and serotonergic alterations. *Toxicol Lett* **152**: 63–71.

Lehmann J, Stohr T, Feldon J (2000) Long-term effects of prenatal stress experiences and postnatal maternal separation on emotionality and attentional processes. *Behav Brain Res* **107**: 133–144.

Lindvall O, McKay R (2003) Evidence for neurogenesis in the adult mammalian substantia nigra. *Proc Natl Acad Sci USA* **100**: 7925–7930.

Marin O, Rubenstein JL (2003) Cell migration in the forebrain. *Annu Rev Neurosci* **26**: 441–483.

Miller MW, Nowakowski RS (1988) Use of bromodeoxyuridine- immunohistochemistry to examine the proliferation, migration and time of origin of cells in the central nervous system. *Brain Res* **457**: 44–52.

Moore SJ, Turnpenny P, Quinn A *et al.* (2000) A clinical study of 57 children with fetal anticonvulsant syndromes. *J Med Genet* **37**: 489–497.

Morris SM (1991) The genetic toxicology of 5-bromodeoxyuridine in mammalian cells. *Mutat Res* **258**: 161–188.

Murphy ML (1965) Dose–response relationships in growth-inhibitory drugs in the rats, time of treatment as a teratological determinant. In: Wilson JG, Warkany J (eds). *Teratology, Principles and Techniques*. University of Chicago Press, Chicago, pp. 161–184.

Nagao T, Saito Y, Watanabe C, Imai K (1997) Reproductive effects of prenatal exposure to 5-bromo-2′-deoxyuridine on male rats. *Reprod Toxicol* **11**: 37–45.

Nagao T, Kuwagata M, Saito Y (1998) Effects of prenatal exposure to 5-bromo-2′-deoxyuridine on the developing brain and reproductive function in male mouse offspring. *Reprod Toxicol* **12**: 477–487.

Ogawa T, Mikuni M, Kuroda Y, Muneoka K, Mori KJ, Takahashi K (1994) Periodic maternal deprivation alters stress response in adult offspring: potentiates the negative feedback regulation of restraint stress-induced adrenocortical response and reduces the frequencies of open field-induced behaviors. *Pharmacol Biochem Behav* **49**: 961–967.

Rogan WJ, Gladen BC, Hung KL *et al.* (1988) Congenital poisoning by polychlorinated biphenyls and their contaminants in Taiwan. *Science* **241**: 334–336.

Ruffolo P, Ferm V (1965) The embryocidal and teratogenic effects of 5-bromodeoxyuridine in the pregnant hamster. *Lab Invest* **14**: 1547–1553.

Schwartz SA, Kirsten WH (1974) Distribution of 5-bromodeoxyuridine in the DNA of rat embryo cells. *Proc Natl Acad Sci USA* **71**: 3570–3574.

Skalko RG, Packard DS, Schwendiman RN, Raggio JF (1971) The teratogenic response of mouse embryos to 5-bromodeoxyuridine. *Teratology* **4**: 87–94.

Soriano E, Del Rio JA (1991) Simultaneous immunocytochemical visualization of bromodeoxyuridine and neural tissue antigens. *J Histochem Cytochem* **39**: 255–263.

Takahashi T, Goto T, Miyama S, Nowakowski RS, Caviness VS Jr (1999) Sequence of neuron origin and neocortical laminar fate: Relation to cell cycle of origin in the developing murine cerebral wall. *J Neurosci* **19**: 10357–10371.

Tamamaki N, Fujimori KE, Takauji R (1997) Origin and route of tangentially migrating neurons in the developing neocortical intermediate zone. *J Neurosci* **17**: 8313–8323.

Webster W, Shimada M, Langman J (1973) Effect of fluorodeoxyuridine, colcemid, and bromodeoxyuridine on developing neocortex of the mouse. *Am J Anat* **137**: 67–85.

Williams G, King J, Cunningham M, Stephan M, Kerr B, Hersh JH (2001) Fetal valproate syndrome and autism: Additional evidence of an association. *Dev Med Child Neurol* **43**: 202–206.

Yamauchi H, Katayama K, Ueno M, Uetsuka K, Nakayama H, Doi K (2004) Involvement of p53 in 1-beta-D-arabinofuranosylcytosine-induced rat fetal brain lesions. *Neurotoxicol Teratol* **26**: 579–586.

Yu WH (1976) The effect of 5-bromodeoxyuridine on the postnatal development of the rat cerebellum: A biochemical study. *Brain Res* **118**: 281–291.

Yu WH (1977) The effect of 5-bromodeoxyuridine on the postnatal development of the rat cerebellum: morphologic and radioautographic studies. *Am J Anat* **150**: 89–107.

Development of functional human embryonic stem cell-derived neurons in mouse brain

Alysson R. Muotri*†, Kinichi Nakashima*†‡, Nicolas Toni*, Vladislav M. Sandler*, and Fred H. Gage*§

*Laboratory of Genetics, The Salk Institute for Biological Studies, 10010 North Torrey Pines Road, La Jolla, CA 92037; and ‡Laboratory of Molecular Neuroscience, Graduate School of Biological Sciences, Nara Institute of Science and Technology, 8916-5 Takayama, Ikoma 630-0101, Japan

Contributed by Fred H. Gage, October 27, 2005

Human embryonic stem cells are pluripotent entities, theoretically capable of generating a whole-body spectrum of distinct cell types. However, differentiation of these cells has been observed only in culture or during teratoma formation. Our results show that human embryonic stem cells implanted in the brain ventricles of embryonic mice can differentiate into functional neural lineages and generate mature, active human neurons that successfully integrate into the adult mouse forebrain. Moreover, this study reveals the conservation and recognition of common signals for neural differentiation throughout mammalian evolution. The chimeric model will permit the study of human neural development in a live environment, paving the way for the generation of new models of human neurodegenerative and psychiatric diseases. The model also has the potential to speed up the screening process for therapeutic drugs.

chimeric model | human ES cells | neuronal differentiation

Human embryonic stem cells (hESC) are known for their ability to propagate indefinitely in culture as undifferentiated cells; furthermore, they can be induced to differentiate *in vitro* and *in vivo* into various cell types (1). However, it is currently unknown whether hESC can differentiate into authentic human neurons *in vivo*. The transplantation of hESC into the developing mouse brain is a valuable model for studying the differentiation and migration potential of hESC *in vivo*. Detailed knowledge about human neural differentiation during development will certainly prove valuable in the regenerative medicine field and in drug discovery. We have investigated this process both *in vitro* and *in vivo*.

Methods

Culture and Differentiation of hESC. The Cyth25 cell line (Cythera, San Diego) was cultured on mitotically inactivated (mitomycin C-treated) mouse embryonic fibroblasts (Specialty Media, Lavellette, NJ) in DMEM/F12 Glutamax (GIBCO), 20% knockout serum replacement (GIBCO), 0.1 mM nonessential amino acids (GIBCO), 0.1 mM 2-mercaptoethanol (GIBCO), and 4 ng/ml bFGF-2 (R & D Systems). hESC neuronal differentiation was obtained by coculture with PA6 cells for 3–5 weeks under the following differentiation conditions: DMEM/F12 Glutamax (GIBCO), 10% knockout serum replacement (GIBCO), 0.1 mM nonessential amino acids (GIBCO), and 0.1 mM 2-mercaptoethanol (GIBCO). Alkaline phosphatase activity was measured by using the Vector Red Alkaline Phosphatase substrate kit I from Vector Laboratories.

hESC Transfection. hESC were stably transfected to express enhanced GFP (EGFP) by CAG-EGFP self-inactivating lentivirus infection. The self-inactivating lentiviral vector expressing EGFP under control of the CAG promoter was derived from a multiply attenuated HIV vector system but included a U3 deletion and introduction of a central polypurine tract element. Vectors were produced by triple transfection of HEK293 cells followed by ultracentrifugation and titration as described in ref. 2. Undifferentiated cells were exposed to the virus at a titer of 0.5×10^{10} gene transfer units/ml for 1 h followed by a 2-day recovery period. EGFP was detected by native fluorescence at day 3 after transduction in ≈1% of the cells. Cells expressing EGFP were manually selected for stable and uniform EGFP expression. Only subtle loss in EGFP expression was observed during propagation or *in vitro* differentiation for up to a year after transduction. The EGFP+ cells derived from these colonies are thus polyclonal in origin and are all positive for human nuclear antigen (hNA). The EGFP+ hESC maintain a phenotype similar to the wild-type cells [stage-specific embryonic antigen (SSEA)-4, terato-related antigen (TRA)-1-60, TRA-1-81, and Pit1-Oct1-Unc86 transcription factor octamer-4 (OCT4)-positive].

***In Utero* hESC Transplantation.** Time-pregnant ICR females were anesthetized, and embryos were removed with intact placenta. Approximately 10^5 EGFP+ hESC in 1 μl of PBS were injected into the lateral ventricle of each embryo (embryonic day 14) with the help of a micro glass capillary and mouth pipette technique. After injection, embryos were placed back into the female with the addition of 1 ml of saline solution. Females were placed in cages, and pups were born by normal vaginal delivery. Weaned animals were kept in individual cages for future experiments. All experiments were performed in compliance with institutional and U.S. National Academies guidelines and with the protocol approved by The Salk Institute Animal Care and Use Committee.

Immunofluorescence. Injected animals were perfused at different time points with 4% paraformaldehyde, and brains were equilibrated in 30% sucrose. Entire brains were processed in 40-μm microtome sections. Immunofluorescence was performed as described by using the following antibodies at the indicated dilutions (3): rabbit anti-β tubulin-III (TUJ1; 1:1,000, Covance, Richmond, CA), guinea pig anti-glial fibrillary acidic protein (1:1,000; Advanced Immunochemical, Long Beach, CA), mouse anti-RIP (1:250, Chemicon), mouse anti-microtubule-associated protein 2(a+b) (1:100, Sigma), mouse anti-S100-β (1:100, Sigma), mouse anti-glutathione transferase π (1:500, BD Pharmingen), mouse anti-OCT4 (1:500, Santa Cruz Biotechnology), and the other marker antibodies, hNA, SSEA-1, SSEA-4, TRA-1-60, TRA-1-81, and Nestin (1:100, Chemicon). All secondary antibodies were purchased from Jackson ImmunoResearch. Fluorescent signals were detected by using a confocal laser scanning head (Bio-Rad MRC 1000) on a Zeiss inverted microscope. Images were processed with PHOTOSHOP 7 (Adobe Systems, San Jose, CA).

Laser Capture. Forty-micrometer microtome sections were immunostained with anti-EGFP antibody (1:500, Chemicon), rapidly

Conflict of interest statement: No conflicts declared.

Abbreviations: hESC, human ES cells; EGFP, enhanced GFP; hNA, human nuclear antigen; SSEA, stage-specific embryonic antigen; TBP, TATA-binding protein.

†A.R.M. and K.N. contributed equally to this work.

§To whom correspondence should be addressed. E-mail: gage@salk.edu.

www.pnas.org/cgi/doi/10.1073/pnas.0509315102

dehydrated through xylenes, and stored until use in a vacuum dessicator. A PixCell II machine (Arcturus, Mountain View, CA) was used to isolate 30 EGFP+ and EGFP− cells from different regions of the brain. Genomic DNA was isolated and prepared as described in ref. 4.

Microscopy. For confocal microscopy, mice were anesthetized 1 and 2 months after injection of EGFP+ hESC and were perfused with 4% paraformaldehyde. Brains were sectioned at a thickness of 100 μm. Dendrites were imaged with a ×40 oil lens and a z-step of 0.5 μm by using a Bio-Rad radiance 2100 confocal microscope. To restrict our study to perforant path inputs, we analyzed the distal portion of the dendritic tree after the first branching point. Seven cells, 15 dendritic segments, and 2,400 protrusions were analyzed. Protrusions were counted on projection images of labeled dendrites. For electron microscopy, mice were anesthetized and perfused with 4% paraformaldehyde plus 0.2% glutaraldehyde. Sections of a thickness of 100 μm were cut, and hESC-derived EGFP+ cells were microinjected under a fluorescence microscope with 5% aqueous lucifer yellow (Aldrich). Slices were then incubated with 2.8 mM 3,3′-diaminobenzidine tetrahydrochloride (DAB) and 6 mM potassium cyanide and then irradiated under conventional epifluorescence by using a 75-W Hg lamp and a fluorescein filter set to induce photoconversion of DAB. Slices were then postfixed overnight in a solution of 3% glutaraldehyde and processed conventionally for electron microscopy. Sections were cut at a thickness of 60 nm and analyzed with a JEOL 100CXII electron microscope at a magnification of ×19,000.

Electrophysiology. Brain slices were prepared as described in refs. 5 and 6. In brief, 18-month-old adult mice were anesthetized with halothane (Ayerst Laboratories) and rapidly decapitated. The brains were immediately harvested and placed into ice-cold cutting solution that consisted of 120 mM choline-Cl, 3 mM KCl, 8 mM $MgCl_2$, 1.25 mM NaH_2PO_4, 26 mM $NaHCO_3$, and 10–20 mM glucose. A vibratome apparatus was used to cut 300-mm-thick slices. After they were cut, slices were kept at room temperature (≈25°C) in artificial cerebrospinal fluid, which was composed of 124 mM NaCl, 2.5 mM KCl, 2 mM $CaCl_2$, 2 mM $MgCl_2$, 1.25 mM NaH_2PO_4, 26 mM $NaHCO_3$, and 10 mM glucose, bubbled with a mixture of 95% O_2/5% CO_2, making the final pH 7.4 (300–315 mOsm/kg). Experiments were performed at room temperature. EGFP-expressing neurons in acute brain slices were identified by using wide-field illumination at 488 nm and emission at 520 nm. Pipettes were sealed on cell bodies by using video-enhanced differential interference contrast optics (7). Intracellular solution contained 130 mM K-methanesulfonate, 4 mM NaCl, 2 mM Mg-ATP, 0.3 mM Na-GTP, and 10 mM Hepes; pH was adjusted to 7.3 with CH_3SO_4 (300 mOsm/kg). Pipette resistance was 5–7 MΩ. Neuronal recordings were made in voltage-clamp mode by using an Axopatch 200B amplifier (Axon Instruments, Foster City, CA). Signals were filtered at 10 kHz. Holding currents were adjusted to 0 pA at the beginning of recording to identify the membrane potential of a neuron. No correction was made for the junction potential between the bath and the pipette. Data are presented as means ± SD. Recorded cells were filled with 5 μM Alexa Fluor 594 (Molecular Probes) through the recording pipette to ascertain that the recorded cell was indeed EGFP+. Alexa Fluor 594 was detected by using wide-field illumination at 595 nm and emission at 615 nm. After recording, slices were fixed in 4% paraformaldehyde for >24 h and then imaged by using a SPOT RT charge-coupled device camera (Diagnostic Instruments, Sterling Heights, MI) to visualize recorded neurons.

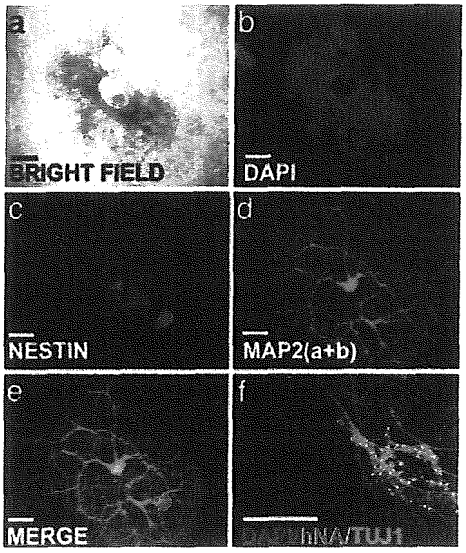

Fig. 1. *In vitro* neuronal differentiation of Cyth25 hESC. (*a*) Example of a differentiated hESC colony after 5 months in PA6 feeder coculture. (*b–d*) DAPI nuclear staining (*b*), Nestin (*c*), and microtubule-associated protein 2(a+b) (*d*). (*e*) Merged image of *c* and *d*. (*f*) Differentiated cells that are positive for TUJ1 colocalize with hNA. (Scale bars, 50 μm.)

Results

Cyth25 hESC were cocultured with mouse embryonic fibroblasts in a defined medium and were immunoreactive for undifferentiated markers, including OCT4, TRA-1-60, TRA-1-81, and SSEA-4, but not for the murine embryonic marker SSEA-1 (see Fig. 5 *a* and *b*, which is published as supporting information on the PNAS web site). In addition, >90% of the colonies showed alkaline phosphatase activity, and most of the cells kept a stable karyotype even at higher passages (>50) (data not shown). Undifferentiated colonies were also positive for a specific hNA (Fig. 5*c*). Moreover, cells were immunonegative for Nestin, a neural precursor marker; TUJ1 and microtubule-associated protein 2(a+b), immature neuronal markers; NeuN, a mature neuronal marker; glial fibrillary acidic protein and S100-β, astrocyte markers; and oligodendrocyte marker 4, glutathione transferase π, and RIP, oligodendrocyte markers (data not shown), suggesting that these cells remained undifferentiated in culture.

The ability of Cyth25 *hESC* to differentiate into neurons was examined by coculture with the mouse skull bone marrow-derived stromal cell line PA6 (8). After 3–4 weeks, most of the colonies became positive for Nestin, and, after 5 weeks, >95% of the colonies formed extensive processes and expressed neuronal markers, such as microtubule-associated protein 2(a+b) (Fig. 1 *a–e*). Neurons generated by this process were immunopositive for hNA (Fig. 1*f*). For transplantation purposes, undifferentiated Cyth25 hESC were infected with the self-inactivating lentivirus carrying the reporter gene *EGFP* (9). Colonies with undifferentiated morphology (round and compact colonies with well defined borders containing cells with a high ratio of nucleus to cytoplasm and prominent nucleoli; see Fig. 5*c*) were selected, isolated by mechanical dissociation, and briefly trypsinized to produce small clumps of cells in suspension. By the time of the transfection, the vast majority of the cells highly expressed the *EGFP* reporter gene. We estimated that ≈10^5 hESC were grafted into the lateral ventricle of embryonic-day-14 ICR mice. The experiment was done in four different pregnant females, and results are summarized in Table 1. Neither teratomas nor tumors were observed at any time. Furthermore, no rejection or immu-

Table 1. Summary of experimental results obtained with hESC transplantation in mouse embryos

Experiment	Cell passage	No. of embryos that died	No. of embryos with good integration	No. of embryos with poor integration	No. of embryos with no integration
1	30	0	7	0	2
2	40	1	4	4	0
3	45	4	1	0	3
4	52	0	1	5	0

Good integration means six or more EGFP+ cells per 40-μm brain section. Poor integration refers to fewer than six EGFP+ cells per 40-μm brain section.

nological reaction was observed, indicating the immunotolerance of the embryonic brain.

Transplanted cells were identified in brain slices by EGFP fluorescence. In the animals with detected incorporated cells, an average of six EGFP+ cells were found in each 40-μm brain microtome section. Despite the high variability observed in different animals, we estimate that <0.1% of the brain cells are of human origin. Most EGFP+ cells colocalized with hNA, and serial 3D reconstruction of confocal sections revealed only one nucleus (Fig. 2*a*). However, we did observe hNA+ cells that were not EGFP+, suggesting that some cells may have their EGFP expression silenced upon differentiation, contrary to what was observed *in vitro* (Fig. 1*f*). A few EGFP+ cells were observed

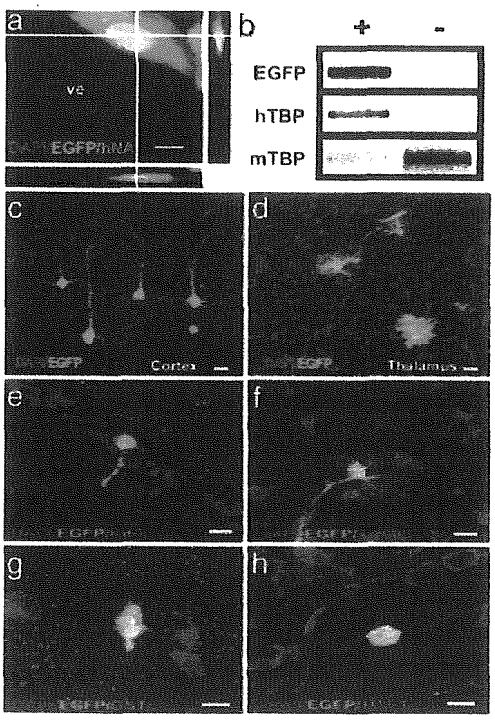

Fig. 2. Widespread chimerism of hESC in the mouse developing brain visualized by EGFP fluorescence. (*a*) 3D reconstruction of 1-μm confocal sections of a hNA+/EGFP+-colabeled cell in the subgranular layer of the ventricular zone (SVZ). ve, ventricle. (*b*) An enriched population (≈200 cells) of laser-captured EGFP (+) cells was PCR-positive for the human-specific TBP sequence (hTBP). The same number of non-EGFP cells (−) was positive only for the mouse sequence (mTBP). (*c* and *d*) Morphological aspect of hESC in different areas of the host brain, such as cortex (*c*) and thalamus (*d*). (*e–h*) *In vivo* neural differentiation of hESC; EGFP+ cells are negative for proliferative markers (such as Ki67; SVZ region in *e*) and express astrocyte (S100-β in the cortex; region in *f*), oligodendrocyte (glutathione transferase π in the hypothalamus; region in *g*) and neuron (Tuj-1; SVZ region in *h*) markers. (Scale bars, 10 μm.)

that did not overlap with the hNA marker and may represent differential antibody accessibility in some differentiated cells. However, laser-captured EGFP+ cells were PCR-positive for the human-specific, single-copy TATA-binding protein (TBP) gene but not for the mouse gene, using specific primers set for each species (10) (Fig. 2*b*). If all of the EGFP+ were fused with mouse cells, the intensities of the mouse TBP band in EGFP+ and EGFP− cells should have been the same; this was clearly not the case. Although we cannot completely exclude the possibility, our results show no evidence of hESC fusion with host cells. Hence, it seems unlikely that fusion plays a dominant role in the observed differentiation of hESC in mouse brain. Two months after transplantation, recipients' brains showed widespread incorporation of hESC in a variety of regions, such as cortex, hippocampus, thalamus, cerebellum, striatum, and corpus callosum, indicating that transplanted cells migrated out from the ventricle into various host brain regions, both ipsilateral and contralateral to the injection site, engrafting at various levels of the neuraxis (Fig. 2 *c* and *d*). A small fraction of the transplanted cells integrated individually or in small clusters into the host tissue with morphometric dimensions similar to those of adjacent host cells, including shape, size, and orientation, and adjusted to the preexisting cellular architecture.

The remaining cells in the host ventricle formed clusters attached to the walls but without apparent consequences for the animals for up to 18 months of age (Fig. 6, which is published as supporting information on the PNAS web site, and Table 1). It is important to note that the integration was not uniform in all animals. Some animals had no or few detectable cells. We hypothesize that this variation is likely due to a variety of reasons including cell number, cell passage, and manipulation or embryonic handling before transplantation. The ventricle-associated cells were weakly immunoreactive for Nestin but negative for cleaved Caspase-3 and Ki67 (Fig. 2*e*). In addition, they did not incorporate BrdUrd by either 7 or 30 days after administration, indicating that they were not in an active proliferative state but remained quiescent (data not shown).

The identity of the incorporated cells was analyzed by immunostaining with specific antibodies for neurons, astrocytes, and oligodendrocytes. Immature neurons (TUJ1+) were found in the subventricular zone (Fig. 2*h*). In the dentate gyrus, NeuN+ cells showed the mature morphological characteristics of granule cells, including dendritic trees extending into the molecular layer and axonal projections into the hilar area, characteristics of native mature neurons in this region (Fig. 3*c*). In addition, transplanted cells that integrated into the hippocampus expressed calbindin, a calcium-binding protein typically found in mature granule neurons (Fig. 7, which is published as supporting information on the PNAS web site). Intriguingly, the diameter of EGFP+/calbindin+ granular cell bodies (11.1 ± 0.6 μm; $n = 5$ in two different animals) was similar to that of mouse cells in the same region (11.1 ± 3.3 μm; $n = 1{,}000$ in two different animals), indicating the ability of the human transplanted cells to adjust their size in relation to adjacent neurons (human granular cell body diameter is, on average, 16.9 ± 3.4 μm; $n = 1{,}000$ in several

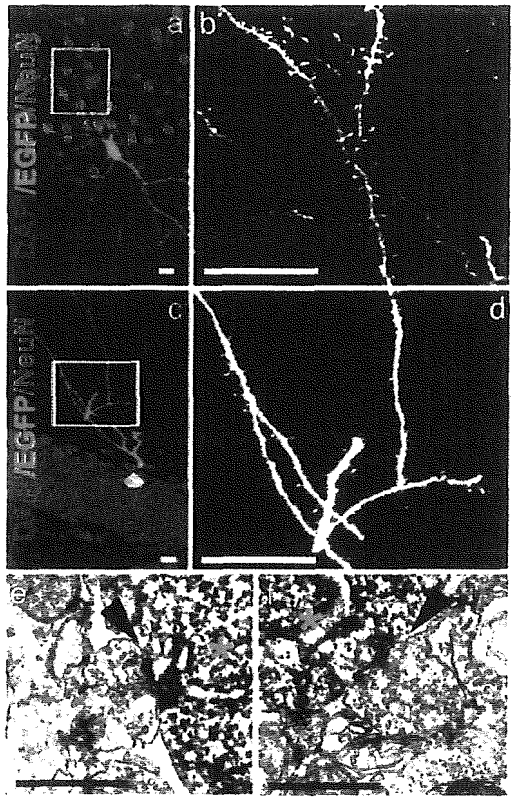

Fig. 3. Maturation of neuron-derived hESC. (*a* and *c*) Visualization of spines in EGFP+/NeuN+ cells in the cortex (*a*) or in the dentate gyrus (*c*) 2 months after transplantation. The boxed areas correspond to the enlarged images of the dendrites in *b* and *d*, respectively. (Scale bars, 10 μm.) (*e* and *f*) Electron micrographs of synaptic terminals (arrowheads) on the soma of EGFP+ neurons (*) in the granule cell layer of the dentate gyrus. (Scale bars, 0.75 μm.)

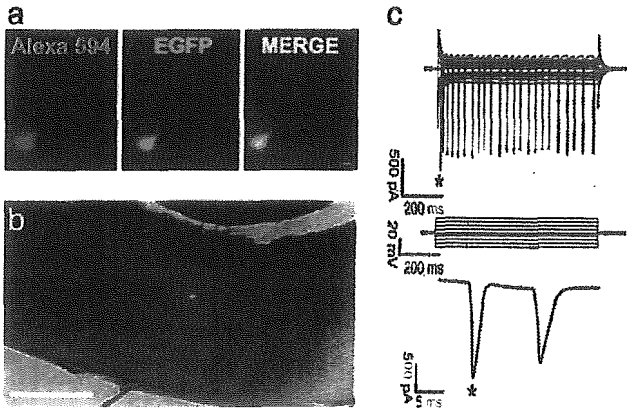

Fig. 4. hESC differentiate into functionally mature neurons in the mouse brain. (*a*) A neuron filled with Alexa Fluor 594 and expressing EGFP. (Scale bar, 20 μm.) (*b*) Low-magnification merge of EGFP, Alexa Fluor 594, and bright-field images shows the position of a recorded neuron in the mouse cortex. (Scale bar, 1 mm.) (*c*) Whole-cell recording from the neuron shown in *a*. The neuron generates a train of action potentials (*Top*) in response to depolarization according to the voltage protocol shown in *Middle*. Time expansion of the first two action potentials is labeled by an asterisk.

samples analyzed). Furthermore, mature neurons in the cortex frequently displayed the morphologies of projection neurons, with pyramidal cell bodies, long apical dendrites reaching into the superficial cortical layers, and basal axons extending into the corpus callosum (Fig. 2*c*).

Evidence of synaptic inputs was apparent in the presence of arborized dendrites with spines, suggesting that glutamate-containing terminals contacted these dendrites (Fig. 3 *b* and *d*). We used confocal microscopy to examine the density of dendritic protrusions on EGFP+ neurons in the granule cell layer. Protrusions at least 0.4 μm in length were included in the counts, and their numbers were divided by the dendritic length to obtain linear density. We obtained a density of 2.5 $\pm$ 0.08 protrusions per micrometer of dendrite, a value comparable to that obtained in adult mouse dentate gyrus (11), indicating that the morphology of EGFP+ neurons is similar to mature neurons and suggesting the presence of glutamatergic inputs. Ultrastructural analysis also confirmed that EGFP+ cells in the granular zone of the dentate gyrus received synaptic input and exhibited mature features, such as pools of presynaptic vesicles adjacent to a postsynaptic density (Fig. 3 *e* and *f*). In humans, granule cells in the hippocampus are formed mainly in the first 4–6 months after birth (12). Interestingly, the transplanted cells could regulate their maturation speed and size within the recipient granular layer, and they established contact with host neurons, revealing remarkable conservation of signaling across these two species.

hESC-derived astrocytes expressed S100-β, showing no difference in size or branching pattern when compared with host cells in the same region (Fig. 2*f*). In addition to neurons and astrocytes, EGFP+ oligodendrocytes were found in the mouse brains with hESC transplants. The identity of these oligodendrocytes was confirmed by glutathione transferase π immunofluorescence. Their size and orientation were indistinguishable from those of their host counterparts (Fig. 2*g*).

To investigate whether mature, hESC-derived neurons are functional even a long time (18 months) after transplantation, electrophysiological recordings of EGFP+ cells from adult animals were made in acute brain slices. Recorded EGFP+ cells ($n = 5$, from two different animals) showed neuronal properties similar to mature pyramidal cortical neurons under comparable recording conditions (13). The membrane potential of the recorded neurons was -64.8 ± 3.1 mV. Membrane resistance was 38.1 ± 3.2 MΩ. The amplitude of the first action potential in a train was $1{,}572 \pm 286$ pA. Two neurons generated a burst of three to four action potentials in response to depolarization (Fig. 4).

Discussion

Our results show that hESC, transplanted into the ventricle of the developing mammalian brain, can give rise to neuronal and glial lineages, suggesting that they are responsive to environmental cues that regulate cell fate determination and differential migration. Access to large areas of the neuroepithelium, the lack of immunological response, and the neurogenically enriched environment of the embryonic brain appear to be responsible for the first steps of hESC-grafted cell differentiation. Donor-derived neurons seem to respond to local differentiation signals, acquiring morphological and functional features similar to host neurons and displaying remarkable regional specificity. Such a contribution to the host tissue formation probably requires a close physical interaction between the transplanted and intrinsic cells.

Depending on the injection site, murine ES cells and teratocarcinoma NT2 cells transplanted to the adult mouse brain frequently develop tumors (14, 15). hESC have been transplanted into immunocompromised adult mice to form teratomas that contain derivatives of the three embryonic germ layers, demonstrating the potency of these cells (1). Interestingly, our

results suggest that transplanted hESC in the embryonic-day-14 mouse ventricle stop dividing and do not form teratomas. Tumor formation seems to be caused by different factors, including the number of viable cells and the age and site of host tissue. In contrast, both murine ES and teratocarcinoma cells have been shown to participate in normal development upon introduction into early embryos at the blastocyst stage (16).

Human undifferentiated embryonic cells were also transplanted into somites of chick embryos of 1.5–2 days of development (17). Surprisingly, transplanted cells could migrate, differentiate, and integrate with host tissues, indicating that the host chick embryonic environment may modulate their differentiation. Recent data suggest that, after transplantation, undifferentiated hESC can survive in the striatum of a rat model of Parkinson's disease (18). This finding indicates that hESC can be used as long-term carriers of therapeutic gene product(s). However, there is no evidence that these cells can functionally integrate into the existing nervous system of the host and contribute to behavioral recovery. Transplantation of human fetal, adult neuronal and hematopoietic stem cells into mouse embryos, and their subsequent contribution to a variety of organs, has been reported (19–23). Moreover, the transplantation of human neural stem cells into fetal monkey brain showed an extensive incorporation and neuronal differentiation (24). hESC-derived neural progenitors were also transplanted into the ventricles of newborn mice and adult rats and showed neural differentiation (25–27). Functional neuronal differentiation, detected by synaptic formation, was obtained from human neural stem cells transplantation into gerbil ischemic brain and mouse spinal-cord-injured models, revealing the potential of human cells to form synaptic connections with other species (28, 29). Together with these studies, the data presented here point to conserved neural differentiation signals from mouse to man.

It will be of interest to extend this approach to other tissues of the embryo, allowing the evaluation of functional differentiation of hESC in specific fetal environments, without the use of ethically controversial blastocyst transplantation. In addition, it will be important to standardize these procedures to assure reliable, reproducible, and, hopefully, quantitative assays in the future. The introduction of hESC-derived neurons and glia into the developing nervous system is a new approach for the study of neurological disorders, mainly in those cases when the animal model does not entirely recapitulate the neurodegenerative process observed in humans, such as in the ataxia telangiectasia syndrome (30). Moreover, the system can be applied to study the neural phenotype of certain human diseases in which individuals die before the development of a functional nervous system. Mouse chimeric models have already produced insights into neurodegenerative diseases such as amyotrophic lateral sclerosis (31). Genetic manipulation of hESC (by recombination or delivery of small interfering RNA) (32, 33) or somatic nuclear transfer (34–36) will allow the generation of a large spectrum of modified donor hESC-derived precursor cells that can then be assayed *in vivo* in a wild-type or mutant recipient brain, producing a mouse–human chimeric nervous system. Such a strategy might allow the direct examination of the effect of potential therapeutic molecules on hESC in a live and functioning nervous system, even in long-term paradigms.

We are in debt to Kevin D'Amour for technical advice with Cyth25 cells and Mark Ellisman at the National Center for Microscopy and Imaging Research at the University of California at San Diego (La Jolla). We thank The Salk Institute administration for the establishment of a non-National Institutes of Health core in the Stem Cell Facility through the support of the Lookout Fund and Mathers Foundation. A.R.M. is supported by the Pew Latin America Fellows, K.N. is supported by the Japan Society for the Promotion of Science Postdoctoral Fellowship for Research Abroad, and N.T. is supported by the International Human Frontier Science Program Organization.

1. Thomson, J. A., Itskovitz-Eldor, J., Shapiro, S. S., Waknitz, M. A., Swiergiel, J. J., Marshall, V. S. & Jones, J. M. (1998) *Science* **282,** 1145–1147.
2. Zufferey, R., Nagy, D., Mandel, R. J., Naldini, L. & Trono, D. (1997) *Nat. Biotechnol.* **15,** 871–875.
3. Gage, F. H., Coates, P. W., Palmer, T. D., Kuhn, H. G., Fisher, L. J., Suhonen, J. O., Peterson, D. A., Suhr, S. T. & Ray, J. (1995) *Proc. Natl. Acad. Sci. USA* **92,** 11879–11883.
4. Millar, D. S., Warnecke, P. M., Melki, J. R. & Clark, S. J. (2002) *Methods* **27,** 108–113.
5. Sandler, V. M. & Barbara, J. G. (1999) *J. Neurosci.* **19,** 4325–4336.
6. Sandler, V. M. & Ross, W. N. (1999) *J. Neurophysiol.* **81,** 216–224.
7. Stuart, G. J. & Sakmann, B. (1994) *Nature* **367,** 69–72.
8. Kawasaki, H., Suemori, H., Mizuseki, K., Watanabe, K., Urano, F., Ichinose, H., Haruta, M., Takahashi, M., Yoshikawa, K., Nishikawa, S., *et al.* (2002) *Proc. Natl. Acad. Sci. USA* **99,** 1580–1585.
9. Miyoshi, H., Blomer, U., Takahashi, M., Gage, F. H. & Verma, I. M. (1998) *J. Virol.* **72,** 8150–8157.
10. Imbert, G., Trottier, Y., Beckmann, J. & Mandel, J. L. (1994) *Genomics* **21,** 667–668.
11. Williams, R. S. & Matthysse, S. (1983) *J. Comp. Neurol.* **215,** 154–164.
12. Seress, L. (1992) *Epilepsy Res. Suppl.* **7,** 3–28.
13. Stuart, G., Schiller, J. & Sakmann, B. (1997) *J. Physiol.* **505,** 617–632.
14. Deacon, T., Dinsmore, J., Costantini, L. C., Ratliff, J. & Isacson, O. (1998) *Exp. Neurol.* **149,** 28–41.
15. Miyazono, M., Lee, V. M. & Trojanowski, J. Q. (1995) *Lab. Invest.* **73,** 273–283.
16. Kleppner, S. R., Robinson, K. A., Trojanowski, J. Q. & Lee, V. M. (1995) *J. Comp. Neurol.* **357,** 618–632.
17. Goldstein, R. S., Drukker, M., Reubinoff, B. E. & Benvenisty, N. (2002) *Dev. Dyn.* **225,** 80–86.
18. Park, S., Kim, E. Y., Ghil, G. S., Joo, W. S., Wang, K. C., Kim, Y. S., Lee, Y. J. & Lim, J. (2003) *Neurosci. Lett.* **353,** 91–94.
19. Brustle, O., Choudhary, K., Karram, K., Huttner, A., Murray, K., Dubois-Dalcq, M. & McKay, R. D. (1998) *Nat. Biotechnol.* **16,** 1040–1044.
20. Lagasse, E., Shizuru, J. A., Uchida, N., Tsukamoto, A. & Weissman, I. L. (2001) *Immunity* **14,** 425–436.
21. Verfaillie, C. M. (2002) *Nat. Immunol.* **3,** 314–317.
22. Tamaki, S., Eckert, K., He, D., Sutton, R., Doshe, M., Jain, G., Tushinski, R., Reitsma, M., Harris, B., Tsukamoto, A., *et al.* (2002) *J. Neurosci. Res.* **69,** 976–986.
23. Uchida, N., Buck, D. W., He, D., Reitsma, M. J., Masek, M., Phan, T. V., Tsukamoto, A. S., Gage, F. H. & Weissman, I. L. (2000) *Proc. Natl. Acad. Sci. USA* **97,** 14720–14725.
24. Ourednik, V., Ourednik, J., Flax, J. D., Zawada, W. M., Hutt, C., Yang, C., Park, K. I., Kim, S. U., Sidman, R. L., Freed, C. R. & Snyder, E. Y. (2001) *Science* **293,** 1820–1824.
25. Zhang, S. C., Wernig, M., Duncan, I. D., Brustle, O. & Thomson, J. A. (2001) *Nat. Biotechnol.* **19,** 1129–1133.
26. Reubinoff, B. E., Itsykson, P., Turetsky, T., Pera, M. F., Reinhartz, E., Itzik, A. & Ben-Hur, T. (2001) *Nat. Biotechnol.* **19,** 1134–1140.
27. Tabar, V., Panagiotakos, G., Greenberg, E. D., Chan, B. K., Sadelain, M., Gutin, P. H. & Studer, L. (2005) *Nat. Biotechnol.* **23,** 601–606.
28. Ishibashi, S., Sakaguchi, M., Kuroiwa, T., Yamasaki, M., Kanemura, Y., Shizuko, I., Shimazaki, T., Onodera, M., Okano, H. & Mizusawa, H. (2004) *J. Neurosci. Res.* **78,** 215–223.
29. Cummings, B. J., Uchida, N., Tamaki, S. J., Salazar, D. L., Hooshmand, M., Summers, R., Gage, F. H. & Anderson, A. J. (2005) *Proc. Natl. Acad. Sci. USA* **102,** 14069–14074.
30. Barlow, C., Hirotsune, S., Paylor, R., Liyanage, M., Eckhaus, M., Collins, F., Shiloh, Y., Crawley, J. N., Ried, T., Tagle, D. & Wynshaw-Boris, A. (1996) *Cell* **86,** 159–171.
31. Clement, A. M., Nguyen, M. D., Roberts, E. A., Garcia, M. L., Boillee, S., Rule, M., McMahon, A. P., Doucette, W., Siwek, D., Ferrante, R. J., *et al.* (2003) *Science* **302,** 113–117.
32. Zwaka, T. P. & Thomson, J. A. (2003) *Nat. Biotechnol.* **21,** 319–321.
33. Tiscornia, G., Singer, O., Ikawa, M. & Verma, I. M. (2003) *Proc. Natl. Acad. Sci. USA* **100,** 1844–1848.
34. Hwang, W. S., Ryu, Y. J., Park, J. H., Park, E. S., Lee, E. G., Koo, J. M., Jeon, H. Y., Lee, B. C., Kang, S. K., Kim, S. J., *et al.* (2004) *Science* **303,** 1669–1674.
35. Hwang, W. S., Lee, B. C., Lee, C. K. & Kang, S. K. (2005) *J. Vet. Sci.* **6,** 87–96.
36. Simerly, C., Navara, C., Hyun, S. H., Lee, B. C., Kang, S. K., Capuano, S., Gosman, G., Dominko, T., Chong, K. Y., Compton, D., *et al.* (2004) *Dev. Biol.* **276,** 237–252.

Histone deacetylase inhibition-mediated neuronal differentiation of multipotent adult neural progenitor cells

Jenny Hsieh*†, Kinichi Nakashima*†‡§, Tomoko Kuwabara*, Eunice Mejia*, and Fred H. Gage*§

*Laboratory of Genetics, The Salk Institute, La Jolla, CA 92037; and ‡Laboratory of Molecular Neuroscience, Graduate School of Biological Sciences, Nara Institute of Science and Technology, 8916-5 Takayama, Ikoma 630-0101, Japan

Contributed by Fred H. Gage, October 15, 2004

It has become apparent that chromatin modification plays a critical role in the regulation of cell-type-specific gene expression. Here, we show that an inhibitor of histone deacetylase, valproic acid (VPA), induced neuronal differentiation of adult hippocampal neural progenitors. In addition, VPA inhibited astrocyte and oligodendrocyte differentiation, even in conditions that favored lineage-specific differentiation. Among the VPA-up-regulated, neuron-specific genes, a neurogenic basic helix–loop–helix transcription factor, *NeuroD*, was identified. Overexpression of *NeuroD* resulted in the induction and suppression of neuronal and glial differentiation, respectively. These results suggest that VPA promotes neuronal fate and inhibits glial fate simultaneously through the induction of neurogenic transcription factors including *NeuroD*.

cell fate specification | chromatin | neural stem cell | valproic acid

Multipotent neural progenitor cells can differentiate into neurons and glial cells (e.g., astrocytes and oligodendrocytes) in the mammalian CNS, but the molecular mechanisms that control their fate specification are not yet fully understood. It is becoming increasingly apparent that chromatin accessibility plays a key role in the transcriptional regulation of cell-type-specific gene expression. In eukaryotic cells, DNA is wrapped around core histones and forms nucleosomes that fold into higher-order chromatin structure (1). Modification of histone N-terminal tails through acetylation or deacetylation can alter the interaction between histones and DNA, serving as a mechanism to regulate gene expression (2–5). Histone acetylation has been established to correlate with gene activation (5). Transcriptional coactivators, such as CREB (cAMP-responsive element-binding protein)-binding protein/p300 and its associated factor, PCAF, have been shown to possess histone acetyltransferase activity (6). Conversely, gene repression is associated with histone deacetylation and transcriptional repressors, such as the nuclear receptor corepressor N-CoR and neuron-restrictive silencer factor/repressor element-1 silencing transcription factor (NRSF/REST), are found in complexes with histone deacetylases (HDACs) (7–9).

Although recent work suggests that HDAC recruitment at target promoters is important for lineage specification in a variety of nonneural cell types (10, 11), there is little understanding of the control of chromatin modification and histone acetylation at a global level in a multipotent neural progenitor cell. The identification of compounds that inhibit HDACs has provided useful tools for studying the connection between global chromatin effects and cell lineage specification.

Valproic acid (VPA; 2-propylpentanoic acid) is an established drug in the long-term treatment of epilepsy (12). Recent experiments in 293T, Neuro2A, and teratocarcinoma F9 cells have demonstrated that VPA can directly inhibit HDAC activity and cause hyperacetylation of histones in these cell lines (13, 14). Furthermore, the HDAC inhibition mediated by VPA has been shown to suppress the growth and increase the differentiation of many different tumor cell lines (12). In addition to its differentiation effects, VPA has been shown to mediate neuronal protection through the activation of signal transduction pathways, such as the extracellular signal-regulated kinase (ERK) pathway (15) and through the inhibition of proapoptotic factors (16). Here, we show that VPA induces neural progenitor cells to differentiate predominantly into neurons and that the effects of VPA are mediated, at least in part, by the neurogenic basic helix–loop–helix (bHLH) transcription factor *NeuroD*.

Materials and Methods

Cell Culture and *in Vitro* Differentiation Analysis. The hippocampal neural progenitor cells isolated from adult female Fisher 344 rats in this study have been characterized in refs. 17 and 18. Differentiation conditions for neurons, oligodendrocytes, and astrocytes were described in ref. 19. For VPA-induction experiments, cells were trypsinized and plated into N2 medium containing either 0.3 or 1 mM VPA (Sigma) for 4 days. In some cultures, 10 μM BrdUrd (Sigma) was added to label dividing cells, and 1 μg/ml propidium iodide or 1 μg/ml Hoechst 33342 (Sigma) were added to label dead cells or all cells, respectively. Trichostatin A (TSA; 100 nM) (Upstate Biotechnology, Lake Placid, NY) and 1 μM sodium butyrate (NaB; Sigma) were added in some cultures as an alternative HDAC inhibitor.

Immunocytochemistry and *in Vitro* Quantification. Cells were fixed with 4% paraformaldehyde, followed by immunocytochemical staining as described in ref. 20. Labeled cells were visualized by using a Nikon E800 upright microscope or a Nikon E600 inverted microscope and a Spot RT charge-coupled device camera (Diagnostic Instruments, Sterling Heights, MI). Quantification of cell phenotypes was with StereoInvestigator (MicroBrightfield, Williston, VT). The following primary antibodies were used: rabbit anti-Tuj1 (1:7,500; Covance, Princeton), mouse anti-microtubule-associated proteins 2a and 2b (MAP2ab; 1:250; Sigma); mouse anti-Rip (1:50; Hybridoma Bank, Iowa City, IA); guinea pig anti-glial fibrillary acidic protein (GFAP; 1:2,500; Advanced Immunochemical, Long Beach, CA); rat anti-BrdUrd (1:400; Accurate Chemicals). The detection of BrdUrd in cultured cells required treatment in 2 M HCL at 37°C for 30 min (20). All experiments were independently replicated at least three times.

Freely available online through the PNAS open access option.

Abbreviations: HDAC, histone deacetylase; VPA, valproic acid; TSA, trichostatin A; NRSF/REST, neuron-restrictive silencer factor/repressor element-1 silencing transcription factor; ERK, extracellular signal-regulated kinase; bHLH, basic helix–loop–helix; NaB, sodium butyrate; MAP2ab, microtubule-associated proteins 2a and 2b; GFAP, glial fibrillary acidic protein; FGF-2, fibroblast growth factor 2; IGF-1, insulin-like growth factor 1; STAT3, signal transducer and activator of transcription 3; BMP-2, bone morphogenetic protein 2; LIF, leukemia inhibitory factor; SGZ, subgranular zone.

†J.H. and K.N. contributed equally to this work.

§To whom correspondence may be addressed. E-mail: gage@salk.edu or kin@bs.naist.jp.

Western Blot Analysis. For Western blots detecting changes in histone acetylation, whole-cell lysates were prepared from neural progenitors cultured in undifferentiated conditions [fibroblast growth factor 2 (FGF-2)] or from differentiating conditions [retinoic acid plus forskolin for neurons, insulin-like growth factor 1 (IGF-1) for oligodendrocytes, and leukemia inhibitory factor (LIF) plus bone morphogenetic protein 2 (BMP-2) for astrocytes]. Antibodies recognizing acetylated and total histones H3 and H4 were all from Upstate Biotechnology: rabbit anti-acetyl H3 (1:10,000), rabbit anti-acetyl H4 (1:100), mouse anti-histone H3 (1:100), and rabbit anti-histone H4 (1:100). Immunoblotting of Akt, ERKs, and signal transducer and activator of transcription 3 (STAT3) were performed as described in ref. 21. The following antibodies from Cell Signaling Technology (Beverly, MA) were used: rabbit anti-phospho-Akt (1:100), rabbit anti-Akt (1:1000), rabbit anti-phospho-p44 and -p42 ERKs (1:1,000), rabbit anti-p44 and -p42 ERKs (1:1,000), rabbit anti-phosphotyrosine-STAT3 (1:500), and mouse anti-STAT3 (1:5000).

Expression Vectors and Neural Progenitor Electroporation. The mouse *NeuroD* cDNA was cloned into the pMY expression vector (22) containing internal ribosome entry site GFP. Electroporation (Amaxa Biosystems, Gaithersburg, MD) was performed according to the manufacturer's protocol, and cells were plated in N2 plus 20 ng/ml FGF-2 for 24 h. To induce differentiation, FGF-2 was withdrawn and replaced with fresh N2 media. FBS (0.5%) was included in all differentiation cultures to enhance survival of cells after electroporation. To induce oligodendrocyte-specific differentiation, electroporated cells were directly plated into insulin-free N2 medium plus 500 ng/ml IGF-1 for 4 days. To induce astrocyte-specific differentiation, 50 ng/ml LIF plus 50 ng/ml BMP-2 was added, and the cells were cultured for 4 days.

RT-PCR. Total RNA was isolated from cell cultures by using RNeasy columns (Qiagen, Valencia, CA). RT-PCR was performed essentially as described in ref. 19. Primer sequences are available upon request.

VPA Analysis *in Vivo*. Adult female Fisher 344 rats received two daily i.p. injections of 300 mg/kg VPA (experimental) or saline (control). VPA was also provided in the drinking water (12 g/liter) for the experimental group. All rats received one daily i.p. injection of 100 mg/kg BrdUrd for 6 consecutive days after the first day. After 14 days, animals were killed, perfused with 4% paraformaldehyde, and processed for BrdUrd immunohistochemical staining as described in refs. 17 and 23. The following antibodies were used: rabbit anti-Tuj1 (1:500), guinea pig anti-GFAP (1:1,000), and rat anti-BrdUrd (1:400). Images were acquired by using a Nikon E800 upright microscope equipped with a 10× objective lens and postprocessed in PHOTOSHOP (Adobe Systems, San Jose, CA). All comparative analyses were focused in the subgranular zone (SGZ) of the dentate gyrus on the same side of matched planes of sections in the dorsal hippocampus. For quantification of BrdUrd-positive and BrdUrd/Tuj1-double positive cells, area counts of the SGZ were performed. In each section, four adjacent fields were sampled, starting from where the upper and lower blades meet.

Results

HDAC Inhibition Induces Neuronal Differentiation. Adult hippocampal neural progenitors were used in this study as a model system to elucidate molecular mechanisms that control fate determination. These cells fulfill the definition of multipotent neural progenitor cells: They self-renew when cultured with basic FGF-2 and can differentiate into neurons, oligodendrocytes, and astrocytes after stimulation with exogenous factors (retinoic acid plus forskolin for neurons, IGF-1 for oligodendrocytes, and LIF plus BMP-2 for astrocytes) (see Fig. 6, which is published as supporting information on the PNAS web site) (17–19).

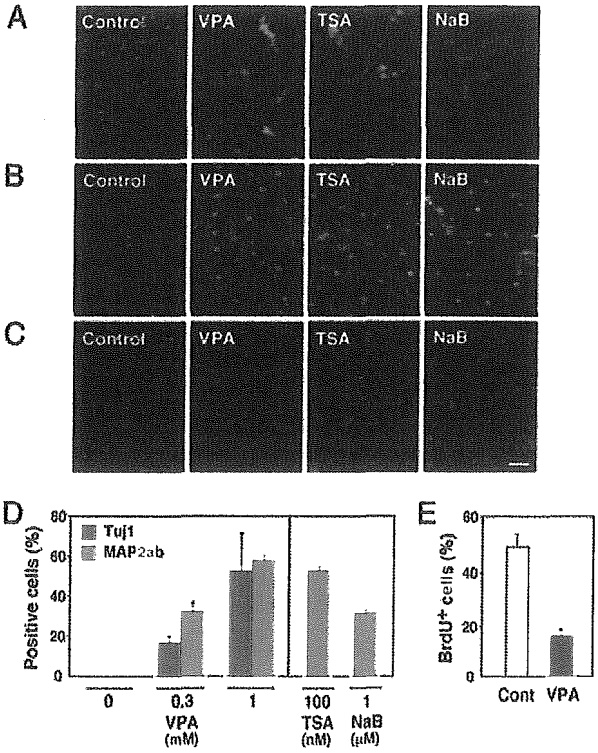

Fig. 1. HDAC-inhibition-mediated neuronal differentiation. (*A*) Treatment of neural progenitors with 1 mM VPA for 4 days resulted in an increase in cells with MAP2ab (green) staining and neuronal morphology compared with control cultures, which lack neuronal differentiation. Similar results were observed with the addition of 100 nM TSA and 1 μM NaB for 2 days. Blue regions indicate 4′,6-diamidino-2-phenylindole-stained nuclei. (*B*) Staining of acetylated histone H3 (red) and MAP2ab (green) is higher in HDAC inhibitor-treated cultures. (*C*) Proliferation in untreated (control) and 1-day HDAC inhibitor-treated cultures as determined by BrdUrd (red) incorporation. (Scale bar, 50 μm.) (*D* and *E*) Quantifications of neuronal differentiation (*D*) and proliferation (*E*) in untreated and HDAC inhibitor-treated cultures. All data shown are from at least three experiments in parallel cultures with error bars representing standard deviations.

To evaluate the functional significance of histone acetylation and deacetylation during multipotent neural progenitor proliferation and differentiation, cell behavior was monitored in the presence of the HDAC inhibitor VPA. Neural progenitors were plated in N2 media with 20 ng/ml FGF-2 for 24 h before switching to fresh N2 medium with or without 1 mM VPA for 4 days (Fig. 1). Lineage-specific differentiation was monitored with markers of neurons (Tuj1 or MAP2ab), oligodendrocytes (Rip), and astrocytes (GFAP). Surprisingly, instead of seeing nonspecific effects on gene expression leading to mixed differentiation of all lineages by VPA treatment, we saw a large increase in Tuj1- and MAP2ab-positive neurons in VPA-treated cultures (Fig. 1 *A* and *D*). The percentage of Tuj1- and MAP2ab-positive neurons was low (<1%) in control cultures (Fig. 1 *A* and *D*). The presence of oligodendrocytes and astrocytes was not detectable in control or VPA-treated cultures (data not shown). Neuronal differentiation by VPA appeared to be dose-dependent (Fig. 1*D*); however, because higher VPA concentrations (>3 mM) resulted in increased cell death, we performed our remaining studies by using concentrations that favored maximal differentiation and minimal toxicity (1 mM VPA; see

Fig. 1*D*). Neural progenitors were also treated with 100 nM TSA and 1 μM NaB, two different HDAC inhibitors that also promoted neuronal differentiation (Fig. 1 *A* and *D*). Because of the higher toxicity of TSA and NaB in neural progenitor cultures, these experiments were carried out for only 2 days.

To verify that VPA, TSA, and NaB were acting as HDAC inhibitors in neural progenitors, we stained control and treated cultures with an antibody specific for acetylated histone H3. Neural progenitors treated with HDAC inhibitors showed increased levels of acetylated histone H3 in the nucleus, compared with untreated neural progenitors (control), suggesting that the increase in neuronal differentiation by VPA, TSA, and NaB was associated with a decrease in HDAC activity (Fig. 1*B*).

To evaluate the effect of HDAC inhibitors on neural progenitor proliferation, neural progenitors in the presence of N2 plus FGF-2 (20 ng/ml) were treated with either VPA, TSA, or NaB or left untreated for 24 h and labeled with 10 μM BrdUrd for 1 h (Fig. 1 *C* and *E*). We observed a dramatic decrease in the percentage of BrdUrd-positive cells in each HDAC inhibitor-treated condition. Approximately 50% of the cells in control cultures were BrdUrd-positive, compared to $\approx$20% of the cells being BrdUrd-positive in VPA-treated cultures (Fig. 1*E*). TSA and NaB also dramatically reduced neural progenitor proliferation (from 50% in control cultures to 8% in treated cultures).

Although the effects of HDAC inhibition in neural progenitors appears mainly to be through a reduction of proliferation and an increase in neuronal differentiation, HDAC inhibitors have also been shown to induce apoptosis (24, 25). We therefore evaluated the degree of cell death in neural progenitor cells by staining living cultures with 1 μg/ml propidium iodide, which stains dead cells, and 1 μg/ml Hoechst 33342, which stains live and dead cells. Staining of live (rather than fixed) cultures was used to avoid underestimating cell death because of the possible detachment of dying and/or dead cells from culture substrates. Neural progenitor cells treated with 1 mM VPA for 2 days resulted in 7.0 $\pm$ 0.1% dead cells, with 25.9% MAP2ab-positive neurons. Cells treated with a lower dose of VPA (0.3 mM) for 2 days resulted in 4.5 $\pm$ 1.6% dead cells, which is only slightly higher than the amount of cell death in untreated control cultures (2.0 $\pm$ 0.1% dead cells). Even with the lower dose of VPA when cell death was minimal, there was still evidence of neuronal differentiation (6.9% MAP2ab-positive cells), suggesting that a selective death of a subset of committed progenitors or nonneuronal cells does not appear to have a significant role in the increased neuronal differentiation with VPA treatment.

Neuronal Lineage Progression Is Associated with Maintenance of Histone Acetylation. To determine whether changes in histone acetylation occur during CNS lineage progression, we compared neural progenitors that had differentiated into neurons, oligodendrocytes, and astrocytes with undifferentiated cells (Fig. 2; see Fig. 6 for each differentiation condition) (19). To detect changes in histone acetylation, protein extracts were harvested from neural progenitors and analyzed by Western blot analysis with antibodies specific for acetylated histones H3 and H4. We detected an abundance of acetylated histones H3 and H4 in extracts of undifferentiated neural progenitors. Interestingly, the level of acetylated histone H3 and H4 was still relatively high in neuronal extracts as compared with undifferentiated extracts, suggesting that there is less deacetylation during neuronal lineage progression. However, there appeared to be less histone H3 and H4 acetylation in astrocyte and oligodendrocyte extracts, suggesting that there is more deacetylation during astrocyte and oligodendrocyte lineage progression compared with neuronal lineage progression (Fig. 2). To exclude the possibility that the changes in histone acetylation observed during CNS lineage progression were due to changes in overall histone levels, we also performed Western blot analysis with antibodies against total

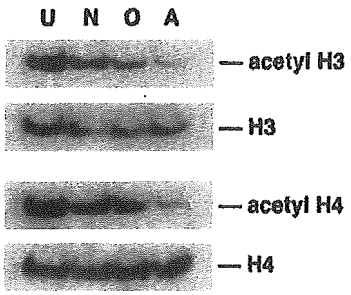

Fig. 2. Changes in histone acetylation during neural progenitor lineage progression. Western blot analysis of neural progenitor extracts from undifferentiated (U) cultures grown in N2 media plus 20 ng/ml FGF-2 or differentiated with 1 μM retinoic acid plus 5 μM forskolin for 4 days (neuron, N), 500 ng/ml IGF-1 for 4 days (oligodendrocyte, O), or 50 ng/ml LIF plus 50 ng/ml BMP-2 for 6 days (astrocyte, A). Immunoblotting was performed by using antibodies against histones H3 and H4 and acetylated histones H3 and H4. Data shown are from at least three independent experiments.

histones. As shown in Fig. 2, the steady-state levels of histones H3 and H4 did not change significantly under various conditions. The observations that VPA treatment increased neuronal differentiation and that the level of acetylated histones was higher in neurons compared with oligodendocytes and astrocytes suggested that histone acetylation is important for neuronal lineage progression of adult multipotent neural progenitor cells. The partial reduction of acetylated histones H3 and H4 in oligodendrocyte and astrocyte extracts suggested that the maintenance of histone acetylation is less important in nonneuronal cells; in fact, there is evidence that recruitment of HDAC activity by the transcriptional regulator NRSF/REST is important to repress the promoter of neuron-specific genes in nonneuronal cells (7, 8, 26). In addition, recent work suggests that histone deacetylase activity is important for oligodendrocyte lineage progression (27).

VPA Actively Suppresses Oligodendrocyte and Astrocyte Differentiation While Promoting Neuronal Differentiation. The decreased histone acetylation in oligodendrocytes and astrocytes suggests that histone deacetylation is important for oligodendrocyte and astrocyte differentiation. To directly test this hypothesis, we induced oligodendrocyte and astrocyte differentiation of neural progenitors in the presence or absence of VPA. IGF-1 (500 ng/ml) induced neural progenitors to differentiate into Rip-positive oligodendrocytes with characteristic web-like processes (Fig. 3) (19). Addition of VPA to IGF-1-treated cultures dramatically reduced the percentage of Rip-positive cells. Intriguingly, the percentage of Tuj1-positive neurons increased in IGF-1-treated cultures when VPA was added. As was seen with neural progenitors that differentiated into astrocytes with 50 ng/ml LIF plus 50 ng/ml BMP-2 (28), addition of VPA reduced the number of GFAP-positive astrocytes and increased the number of Tuj1-positive neurons (Fig. 3). Taken together, these results suggest that histone deacetylation is important for both oligodendrocyte and astrocyte lineage progression, and increased histone acetylation is associated with neuronal lineage progression.

Up-Regulation of HDAC-Dependent, Neuron-Specific Genes After VPA Treatment. The protein NRSF/REST binds to the neuron-restrictive silencer element sequence to mediate transcriptional repression of target genes by the recruitment and association at its N terminus of the mSin3A/HDAC1,2 complex (8, 26). Recent work examined the role of HDAC-dependent repression of neuron-restrictive silencer element-containing, neuron-specific genes and showed that treatment of Rat-1 fibroblasts with the

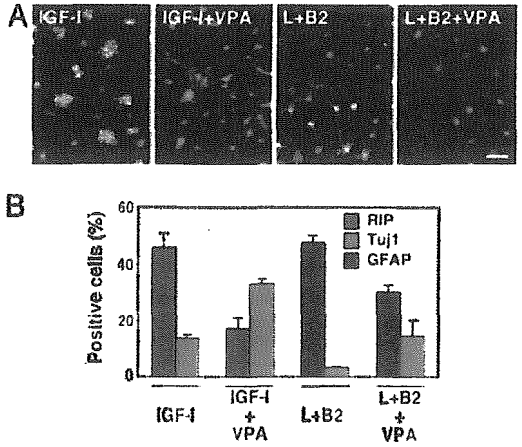

Fig. 3. VPA-mediated suppression of glial differentiation. (*A*) Neural progenitors induced to differentiate into Rip-positive oligodendrocytes (red) with 500 ng/ml IGF-1 or GFAP-positive astrocytes (red) with 50 ng/ml LIF (L) plus 50 ng/ml BMP-2 (B2). Treatment of cultures with 1 mM VPA for 4 days reduced the number of Rip-positive cells (red) in IGF-1-treated cultures and GFAP-positive cells (red) in LIFplusBMP-2-treated cultures, while increasing the number of Tuj1-positive cells (green) in each case. (Scale bar, 50 μm.) (*B*) Quantification of neurons, oligodendrocytes, and astrocytes in various differentiation conditions in the presence or absence of 1 mM VPA. All data shown are from at least three experiments in parallel cultures with error bars representing standard deviations.

HDAC inhibitor TSA resulted in the ectopic activation of a number of neuron-specific genes (29). We therefore performed RT-PCR analysis of HDAC-dependent, neuron-specific genes after VPA treatment (Fig. 4*A*). We could detect an up-regulation of *NeuroD*, *SCG10*, and *Synapsin I* as early as 3 h and at 24 h after VPA treatment. GAPDH levels did not change after VPA treatment and was used as an internal control.

The molecular basis of the reduced proliferation in VPA-treated neural progenitor cells was also examined. Cell cycle regulators, such as cyclin-dependent kinase (CDK) inhibitors, have been shown to be important for the antiproliferative effects of HDAC inhibitors (30, 31). Consistent with this finding, we found that there was increased expression of CDK inhibitors $p21^{WAF1/CIP1}$ and $p27^{KIP1}$ in neural progenitors after VPA treatment (data not shown). These results suggest that neuronal differentiation mediated by VPA involves an up-regulation of both neuron-specific genes and CDK inhibitors to reduce cell proliferation and promote neuronal fate commitment.

It was recently reported that VPA could phosphorylate and activate ERKs 1 and 2, resulting in the differentiation of E18 cortical neurons (32). To determine whether VPA-mediated neuronal differentiation in adult hippocampal neural progenitors was directly caused by the activation of the ERK pathway, we performed a Western blot time-course analysis. Although we did not see ERK activation by VPA after 1 h (Fig. 7 and *Supporting Text*, which are published as supporting information on the PNAS web site), we decided to carry out the experiment for longer time points. Neural progenitor cells were treated with 1 mM VPA, 1 mM valpromide (a VPA analog that is not a HDAC inhibitor, but is also an antiepileptic), and 100 nM TSA for the indicated times (0, 10, and 30 min and 2, 6, and 24 h) and extracts were collected for Western blots (Fig. 4*B*). Although neural progenitors treated with VPA did not show an increase in ERK activation at the earlier time points, there was ERK activation by 24 h. Interestingly, we did not observe ERK activation with TSA or valpromide. To determine whether ERK activation by VPA at 24 h was necessary to trigger neuronal fate commitment, we decided to block ERK activation with an

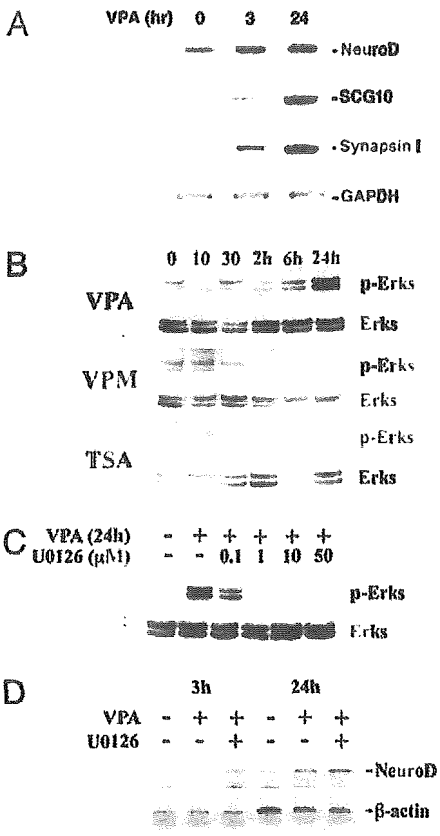

Fig. 4. VPA up-regulates neuron-specific genes, including the bHLH transcription factor *NeuroD*. (*A*) RT-PCR of *NeuroD*, *SCG10*, and *Synapsin I* in neural progenitors at time 0 or treated with 1 mM VPA for 3 h and 24 h. GAPDH was used as a normalization control. (*B*) Western blot time-course analysis of ERK activation after 1 mM VPA, 100 nM TSA, and 1 mM valpromide (VPM) treatment. (*C*) ERK activation with 1 mM VPA treatment with and without addition of U0126 (different doses are indicated). (*D*) RT-PCR analysis of VPA-mediated up-regulation of *NeuroD* (3 and 24 h) with and without U0126 (1 μM).

inhibitor of mitogen-activated protein kinase kinase 1/2 (U0126), which is the upstream kinase that phosphorylates ERKs. Cells were pretreated with control (DMEM/F12 media) or 0.1–50 μM U0126 for 2 h and treated with or without 1 mM VPA for 24 h (Fig. 4*C*). We found that 1 μM U0126 was sufficient to block the ERK activation by VPA at 24 h. We next examined whether neuronal fate commitment mediated by VPA, as evidenced by an up-regulation of the bHLH transcription factor *NeuroD*, could still occur, even when ERK activation was blocked. Cells were pretreated with 1 μM U0126 for 2 h before adding 1 mM VPA for 3 or 24 h (Fig. 4*D*). RT-PCR analysis confirmed that there was up-regulation of *NeuroD* after VPA treatment at 3 h, with even higher levels at 24 h (compared with untreated cells). More importantly, blocking ERK activation did not appear to inhibit the VPA-mediated up-regulation of *NeuroD*, suggesting that ERK activation was not necessary to trigger neuronal differentiation.

The Mechanism of VPA-Mediated Neuronal Differentiation Is Associated with the Activation of *NeuroD*. Among the HDAC-dependent neuron-specific genes that became up-regulated with VPA treatment, *NeuroD* was the best candidate for triggering neuronal fate commitment and promoting differentiation. Strikingly, mice deficient for *NeuroD* completely lack the dentate gyrus granule cell layer, supporting the role of *NeuroD* in the proliferation,

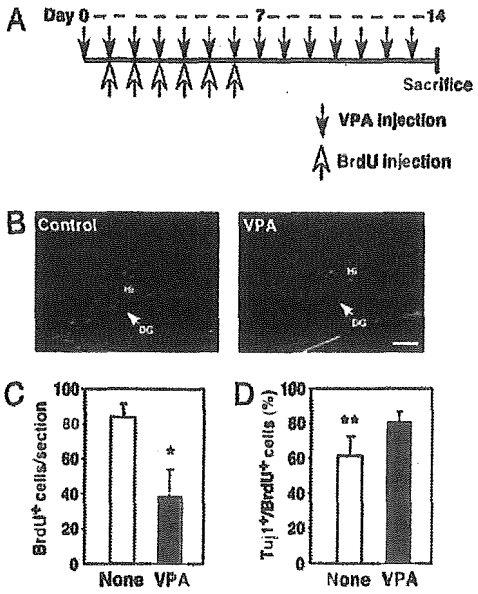

Fig. 5. VPA decreases granule cell proliferation and increases neuronal differentiation in the dentate gyrus of adult rats. (*A*) Schematic of VPA and BrdUrd injection paradigm. (*B*) Representative images of brain sections focusing on the dentate gyrus (DG) of animals injected with saline (control) or VPA. Sections were processed for BrdUrd staining. White arrow indicates the dentate gyrus. Hi, Hilus. (Scale bar, 200 μm.) (*C*) The average number of BrdUrd-positive cells (in four adjacent fields) per section (control animals, $n = 4$; VPA-treated animals, $n = 6$) is plotted. The asterisk indicates that values are significantly different between control and VPA-treated animals ($P < 0.001$, t test). (*D*) The percentage of Tuj1-/BrdUrd-double positive cells (in four adjacent fields) per section (control animals, $n = 4$; VPA-treated animals, $n = 6$) is plotted. Asterisks indicate statistical significance ($P < 0.05$, t test). Error bars represent standard deviations.

differentiation, and survival of granule cells in the hippocampus (33, 34). We therefore examined whether forced expression of *NeuroD* alone could have effects on neuronal differentiation (Fig. 8, which is published as supporting information on the PNAS web site). We found that neural progenitors overexpressing *NeuroD* differentiated into >75% Tuj1-positive and MAP2ab-positive neurons, respectively, and reduced their ability to differentiate into oligodendrocytes and astrocytes under appropriate conditions (Fig. 8). These results suggest that *NeuroD* by itself can recapitulate many of the effects of VPA and is sufficient to induce neuronal differentiation of adult multipotent neural progenitor cells.

VPA-Mediated Neuronal Differentiation *in Vivo*. Our findings raise the question of whether the effects of VPA on adult hippocampal neural progenitors *in vitro* are related to the clinical indications of VPA as an antiepileptic *in vivo*. Pilocarpine-induced status epilepticus increases cell proliferation in the SGZ of the adult dentate gyrus (35). Prolonged seizure activity has also been shown to markedly increase dentate granule cell neurogenesis (35). To examine the potential effects of VPA on dentate granule cell proliferation and neurogenesis, we injected adult rats with VPA for a total of 14 days, while including a 6-day BrdUrd regimen to label dividing cells (Fig. 5*A*). Consistent with previous studies (35), BrdUrd immunohistochemistry in saline-injected rats (controls, $n = 4$) labeled mitotically active cells mostly located in the SGZ of the dentate gyrus (Fig. 5*B*, white arrows). In contrast, VPA-injected rats ($n = 6$) showed a marked reduction in BrdUrd incorporation in the SGZ (Fig. 5*B*, white arrows). No obvious differences in BrdUrd immunostaining were observed in the hilar region or the molecular layer of the dentate gyrus. Quantitative analysis of BrdUrd labeling within the SGZ revealed a significant decrease (≈2-fold) ($P < 0.001$, t test) in the number of dividing cells in VPA-injected rats compared with controls (Fig. 5*C*). The VPA-mediated decrease in granule cell proliferation within the SGZ is consistent with the effects of VPA in decreasing proliferation of neural progenitors *in vitro*.

We next examined the fate of dividing cells in the SGZ by assessing colocalization of BrdUrd with lineage-specific markers (Tuj1 for neurons and GFAP for astrocytes) (Fig. 5*D*). In control animals, ≈60% of the BrdUrd-positive cells were also Tuj1-positive. There was a significant increase (from 60% to 80%) in the percentage of BrdUrd-positive cells that were Tuj1-positive in VPA-treated animals ($P < 0.05$, t test), suggesting that VPA can mediate an increase in neuronal differentiation *in vivo* as well. The percentage of BrdUrd-positive cells that were also GFAP-positive was relatively low (≈1%) in control animals and did not significantly change compared with VPA-treated animals (data not shown). These results support the ability of VPA to decrease neural progenitor proliferation and increase neuronal differentiation *in vivo* as well as *in vitro*.

Discussion

In this series of experiments, we used a well established model system of adult multipotent neural progenitor cells to investigate the connection between global histone acetylation and neural cell fate specification. When cells are cultured in the presence of HDAC inhibitors, such as VPA, TSA, or NaB, neural progenitors reduced their proliferation and largely differentiated into neurons. These findings were also confirmed in our *in vivo* experiments. When neural progenitors were treated with conditions that promoted astrocyte and oligodendrocyte differentiation, VPA actively suppressed differentiation into astrocytes and oligodendrocytes while promoting differentiation into neurons. Analysis of the mechanism of VPA-mediated neuronal differentiation revealed an up-regulation of the neurogenic bHLH transcription factor *NeuroD* in VPA-treated cultures. Furthermore, overexpression of *NeuroD* alone in neural progenitors could recapitulate the effects of VPA.

We and others have previously shown that IGF-1 induces oligodendrocyte differentiation (19) and LIF induces astrocyte differentiation (36, 37). The VPA-mediated suppression of oligodendrocyte and astrocyte differentiation could be due to an inhibition of IGF-1 and LIF signal transduction pathways. Two of the major downstream mediators of IGF-1 signaling are the phosphoinositide 3-kinase/Akt and Ras/ERK pathways (38, 39), and the major downstream mediator of LIF signaling is the Janus tyrosine kinase/STAT pathway (36, 37). First, we did not detect an activation of Akt/ERKs or STAT3 with VPA treatment alone, at least within 1 h (see Fig. 7). Second, the activation status of Akt/ERKs or STAT3 after IGF-1 or LIF stimulation did not change in VPA-treated cultures compared with control cultures. This finding suggests that the VPA-mediated neuronal differentiation and suppression of glial differentiation was not due to a direct activation or inhibition, respectively, of these signaling molecules and point to another mechanism of VPA action.

Recently, Hao *et al.* (32) described the effects of VPA on the activation of the ERK pathway in E18 cortical neurons. In their assay system, VPA promoted neurite growth and cell reemergence in an ERK pathway-dependent manner. Although we were unable to detect an activation of ERKs within 1 h, we did observe ERK activation by VPA after 24 h. However, when we blocked ERK activation with U0126, we were still able to detect an up-regulation of *NeuroD* (at 3 and 24 h), suggesting that neuronal fate commitment triggered by VPA is not directly due to an activation of the ERK pathway. Furthermore, the observation

that TSA was not able to activate ERKs but was able to up-regulate *NeuroD* (data not shown) and promote neuronal differentiation further confirmed that direct activation of the ERK pathway is not solely responsible for neuronal differentiation of adult neural progenitor cells.

An alternative mechanism of the neuron-promoting effect of VPA could be the direct activation of neurogenic transcription factors. Our work indicates that VPA treatment up-regulates *NeuroD* in neural progenitor cells, suggesting that VPA could, in fact, induce neuronal differentiation through the transcriptional activation of neurogenic transcription factors. Lunyak *et al.* (29) showed that the expression of *NeuroD* and of other neuron-specific genes is regulated by the HDAC-dependent transcriptional repressor NRSF/REST. Further examination of other neuron-specific genes, such as *Synapsin I* and *SCG10,* showed that each had increased gene expression after VPA treatment, consistent with previous reports (29). In addition to up-regulating NRSF/REST-regulated neuron-specific genes, VPA up-regulates neuronal markers, such as Tuj1 and MAP2ab, which are not direct targets of NRSF/REST. This finding suggests that the mechanism of VPA-mediated neuronal differentiation is not solely due to a direct release of NRSF/REST repression of neuron-specific genes and that VPA must activate factors important for neuronal lineage progression. The observation that forced expression of *NeuroD* alone can promote neuronal differentiation indicates that VPA may exert its effects through the activation of *NeuroD*. More studies are needed to determine whether the up-regulation of *NeuroD* after VPA treatment is merely correlative or whether there is a causal relationship between the VPA-mediated neuronal differentiation and neurogenic bHLH transcription factors.

Adult multipotent neural progenitor cells need to choose between self-renewal and differentiation into neurons, oligodendrocytes, or astrocytes. We hypothesized that chromatin modification plays an important role in these stem cell decisions because of its ability to control the simultaneous expression of many genes. The observation that VPA can have a profound effect on promoting neuronal differentiation and suppressing glial differentiation suggests that the maintenance of the acetylated state, revealed by HDAC inhibition, may have global and dominant effects on neuronal lineage progression.

Examination of total acetylated histones H3 and H4 in neural progenitor extracts under various conditions revealed that histone acetylation levels were highest in the undifferentiated state. Interestingly, among the differentiation conditions examined, acetylated histone levels were higher in neuronal extracts relative to astrocytic extracts. The level of acetylated histones in oligodendrocytic extracts was always intermediate to that of neurons and astrocytes, possibly because of a partial requirement of histone acetylation for oligodendrocyte lineage progression or the presence of neurons in oligodendrocyte cultures. In fact, a previous study showed that treatment of neural progenitors with IGF-1 (the oligodendrocyte-promoting condition) can also result in a low percentage of Tuj1-positive neurons (Fig. 6) (19). These results support the idea that there are global changes in chromatin states underlying differences in adult multipotent neural progenitor differentiation. Does acetylation of chromatin selectively activate specific master control genes, such as *NeuroD*, that go on to trigger downstream genes important for neuronal differentiation, or does *NeuroD* itself possess the ability to regulate global chromatin-based events, such as the maintenance of histone acetylation? Future studies are needed to determine the precise order and relationship of chromatin modification and the regulation of gene expression in the control of adult multipotent neural progenitor cell fate specification.

We thank M. L. Gage for editorial comments. This work was supported in part by grants from the National Institutes of Health, the George E. Hewitt Foundation for Medical Research, Project A.L.S., the Christopher Reeve Paralysis Foundation, the Pritzker Neurogenesis Research Consortium, and a Japan Society for the Promotion of Science Postdoctoral Fellowship for Research Abroad.

1. Georgopoulos, K. (2002) *Nat. Rev. Immunol.* **2,** 162–174.
2. Grunstein, M. (1997) *Nature* **389,** 349–352.
3. Kuo, M. H. & Allis, C. D. (1998) *BioEssays* **20,** 615–626.
4. Struhl, K. (1998) *Genes Dev.* **12,** 599–606.
5. Jenuwein, T. & Allis, C. D. (2001) *Science* **293,** 1074–1080.
6. Chan, H. M. & La Thangue, N. B. (2001) *J. Cell Sci.* **114,** 2363–2373.
7. Huang, Y., Myers, S. J. & Dingledine, R. (1999) *Nat. Neurosci.* **2,** 867–872.
8. Jepsen, K., Hermanson, O., Onami, T. M., Gleiberman, A. S., Lunyak, V., McEvilly, R. J., Kurokawa, R., Kumar, V., Liu, F., Seto, E., *et al.* (2000) *Cell* **102,** 753–763.
9. Kao, H. Y., Downes, M., Ordentlich, P. & Evans, R. M. (2000) *Genes Dev.* **14,** 55–66.
10. Zhang, C. L., McKinsey, T. A., Chang, S., Antos, C. L., Hill, J. A. & Olson, E. N. (2002) *Cell* **110,** 479–488.
11. Koipally, J., Renold, A., Kim, J. & Georgopoulos, K. (1999) *EMBO J.* **18,** 3090–3100.
12. Blaheta, R. A. & Cinatl, J., Jr. (2002) *Med. Res. Rev.* **22,** 492–511.
13. Gottlicher, M., Minucci, S., Zhu, P., Kramer, O. H., Schimpf, A., Giavara, S., Sleeman, J. P., Lo Coco, F., Nervi, C., Pelicci, P. G. & Heinzel, T. (2001) *EMBO J.* **20,** 6969–6978.
14. Phiel, C. J., Zhang, F., Huang, E. Y., Guenther, M. G., Lazar, M. A. & Klein, P. S. (2001) *J. Biol. Chem.* **276,** 36734–36741.
15. Coyle, J. T. & Duman, R. S. (2003) *Neuron* **38,** 157–160.
16. Perez, M., Rojo, A. I., Wandosell, F., Diaz-Nido, J. & Avila, J. (2003) *Biochem. J.* **372,** 129–136.
17. Gage, F. H., Coates, P. W., Palmer, T. D., Kuhn, H. G., Fisher, L. J., Suhonen, J. O., Peterson, D. A., Suhr, S. T. & Ray, J. (1995) *Proc. Natl. Acad. Sci. USA* **92,** 11879–11883.
18. Palmer, T. D., Takahashi, J. & Gage, F. H. (1997) *Mol. Cell Neurosci.* **8,** 389–404.
19. Hsieh, J., Aimone, J. B., Kaspar, B. K., Kuwabara, T., Nakashima, K. & Gage, F. H. (2004) *J. Cell Biol.* **164,** 111–122.
20. Palmer, T. D., Markakis, E. A., Willhoite, A. R., Safar, F. & Gage, F. H. (1999) *J. Neurosci.* **19,** 8487–8497.
21. Nakashima, K., Narazaki, M. & Taga, T. (1997) *FEBS Lett.* **401,** 49–52.
22. Misawa, K., Nosaka, T., Morita, S., Kaneko, A., Nakahata, T., Asano, S. & Kitamura, T. (2000) *Proc. Natl. Acad. Sci. USA* **97,** 3062–3066.
23. Kempermann, G., Kuhn, H. G. & Gage, F. H. (1997) *Nature* **386,** 493–495.
24. Tang, X. X., Robinson, M. E., Riceberg, J. S., Kim, D. Y., Kung, B., Titus, T. B., Hayashi, S., Flake, A. W., Carpentieri, D. & Ikegaki, N. (2004) *Clin. Cancer Res.* **10,** 5837–5844.
25. Phillips, A., Bullock, T. & Plant, N. (2003) *Toxicology* **192,** 219–227.
26. Naruse, Y., Aoki, T., Kojima, T. & Mori, N. (1999) *Proc. Natl. Acad. Sci. USA* **96,** 13691–13696.
27. Marin-Husstege, M., Muggironi, M., Liu, A. & Casaccia-Bonnefil, P. (2002) *J. Neurosci.* **22,** 10333–10345.
28. Nakashima, K., Yanagisawa, M., Arakawa, H., Kimura, N., Hisatsune, T., Kawabata, M., Miyazono, K. & Taga, T. (1999) *Science* **284,** 479–482.
29. Lunyak, V. V., Burgess, R., Prefontaine, G. G., Nelson, C., Sze, S. H., Chenoweth, J., Schwartz, P., Pevzner, P. A., Glass, C., Mandel, G. & Rosenfeld, M. G. (2002) *Science* **298,** 1747–1752.
30. Archer, S. Y., Meng, S., Shei, A. & Hodin, R. A. (1998) *Proc. Natl. Acad. Sci. USA* **95,** 6791–6796.
31. Vaziri, C., Stice, L. & Faller, D. V. (1998) *Cell Growth Differ.* **9,** 465–474.
32. Hao, Y., Creson, T., Zhang, L., Li, P., Du, F., Yuan, P., Gould, T., Manji, H. & Chen, G. (2004) *J. Neurosci.* **24,** 6590–6599.
33. Miyata, T., Maeda, T. & Lee, J. E. (1999) *Genes Dev.* **13,** 1647–1652.
34. Liu, M., Pleasure, S. J., Collins, A. E., Noebels, J. L., Naya, F. J., Tsai, M. J. & Lowenstein, D. H. (2000) *Proc. Natl. Acad. Sci. USA* **97,** 865–870.
35. Parent, J. M., Yu, T. W., Leibowitz, R. T., Geschwind, D. H., Sloviter, R. S. & Lowenstein, D. H. (1997) *J. Neurosci.* **17,** 3727–3738.
36. Bonni, A., Sun, Y., Nadal-Vicens, M., Bhatt, A., Frank, D. A., Rozovsky, I., Stahl, N., Yancopoulos, G. D. & Greenberg, M. E. (1997) *Science* **278,** 477–483.
37. Takizawa, T., Nakashima, K., Namihira, M., Ochiai, W., Uemura, A., Yanagisawa, M., Fujita, N., Nakao, M. & Taga, T. (2001) *Dev. Cell* **1,** 749–758.
38. LeRoith, D., Werner, H., Beitner-Johnson, D. & Roberts, C. T., Jr. (1995) *Endocr. Rev.* **16,** 143–163.
39. Kulik, G., Klippel, A. & Weber, M. J. (1997) *Mol. Cell. Biol.* **17,** 1595–1606.

Development of functional human embryonic stem cell-derived neurons in mouse brain

Alysson R. Muotri*†, Kinichi Nakashima*†‡, Nicolas Toni*, Vladislav M. Sandler*, and Fred H. Gage*§

*Laboratory of Genetics, The Salk Institute for Biological Studies, 10010 North Torrey Pines Road, La Jolla, CA 92037; and ‡Laboratory of Molecular Neuroscience, Graduate School of Biological Sciences, Nara Institute of Science and Technology, 8916-5 Takayama, Ikoma 630-0101, Japan

Contributed by Fred H. Gage, October 27, 2005

Human embryonic stem cells are pluripotent entities, theoretically capable of generating a whole-body spectrum of distinct cell types. However, differentiation of these cells has been observed only in culture or during teratoma formation. Our results show that human embryonic stem cells implanted in the brain ventricles of embryonic mice can differentiate into functional neural lineages and generate mature, active human neurons that successfully integrate into the adult mouse forebrain. Moreover, this study reveals the conservation and recognition of common signals for neural differentiation throughout mammalian evolution. The chimeric model will permit the study of human neural development in a live environment, paving the way for the generation of new models of human neurodegenerative and psychiatric diseases. The model also has the potential to speed up the screening process for therapeutic drugs.

chimeric model | human ES cells | neuronal differentiation

Human embryonic stem cells (hESC) are known for their ability to propagate indefinitely in culture as undifferentiated cells; furthermore, they can be induced to differentiate *in vitro* and *in vivo* into various cell types (1). However, it is currently unknown whether hESC can differentiate into authentic human neurons *in vivo*. The transplantation of hESC into the developing mouse brain is a valuable model for studying the differentiation and migration potential of hESC *in vivo*. Detailed knowledge about human neural differentiation during development will certainly prove valuable in the regenerative medicine field and in drug discovery. We have investigated this process both *in vitro* and *in vivo*.

Methods

Culture and Differentiation of hESC. The Cyth25 cell line (Cythera, San Diego) was cultured on mitotically inactivated (mitomycin C-treated) mouse embryonic fibroblasts (Specialty Media, Lavellette, NJ) in DMEM/F12 Glutamax (GIBCO), 20% knockout serum replacement (GIBCO), 0.1 mM nonessential amino acids (GIBCO), 0.1 mM 2-mercaptoethanol (GIBCO), and 4 ng/ml bFGF-2 (R & D Systems). hESC neuronal differentiation was obtained by coculture with PA6 cells for 3–5 weeks under the following differentiation conditions: DMEM/F12 Glutamax (GIBCO), 10% knockout serum replacement (GIBCO), 0.1 mM nonessential amino acids (GIBCO), and 0.1 mM 2-mercaptoethanol (GIBCO). Alkaline phosphatase activity was measured by using the Vector Red Alkaline Phosphatase substrate kit I from Vector Laboratories.

hESC Transfection. hESC were stably transfected to express enhanced GFP (EGFP) by CAG-EGFP self-inactivating lentivirus infection. The self-inactivating lentiviral vector expressing EGFP under control of the CAG promoter was derived from a multiply attenuated HIV vector system but included a U3 deletion and introduction of a central polypurine tract element. Vectors were produced by triple transfection of HEK293 cells followed by ultracentrifugation and titration as described in ref. 2. Undifferentiated cells were exposed to the virus at a titer of 0.5×10^{10} gene transfer units/ml for 1 h followed by a 2-day recovery period. EGFP was detected by native fluorescence at day 3 after transduction in ≈1% of the cells. Cells expressing EGFP were manually selected for stable and uniform EGFP expression. Only subtle loss in EGFP expression was observed during propagation or *in vitro* differentiation for up to a year after transduction. The EGFP+ cells derived from these colonies are thus polyclonal in origin and are all positive for human nuclear antigen (hNA). The EGFP+ hESC maintain a phenotype similar to the wild-type cells [stage-specific embryonic antigen (SSEA)-4, terato-related antigen (TRA)-1-60, TRA-1-81, and Pit1-Oct1-Unc86 transcription factor octamer-4 (OCT4)-positive].

***In Utero* hESC Transplantation.** Time-pregnant ICR females were anesthetized, and embryos were removed with intact placenta. Approximately 10^5 EGFP+ hESC in 1 μl of PBS were injected into the lateral ventricle of each embryo (embryonic day 14) with the help of a micro glass capillary and mouth pipette technique. After injection, embryos were placed back into the female with the addition of 1 ml of saline solution. Females were placed in cages, and pups were born by normal vaginal delivery. Weaned animals were kept in individual cages for future experiments. All experiments were performed in compliance with institutional and U.S. National Academies guidelines and with the protocol approved by The Salk Institute Animal Care and Use Committee.

Immunofluorescence. Injected animals were perfused at different time points with 4% paraformaldehyde, and brains were equilibrated in 30% sucrose. Entire brains were processed in 40-μm microtome sections. Immunofluorescence was performed as described by using the following antibodies at the indicated dilutions (3): rabbit anti-β tubulin-III (TUJ1; 1:1,000, Covance, Richmond, CA), guinea pig anti-glial fibrillary acidic protein (1:1,000; Advanced Immunochemical, Long Beach, CA), mouse anti-RIP (1:250, Chemicon), mouse anti-microtubule-associated protein 2(a+b) (1:100, Sigma), mouse anti-S100-β (1:100, Sigma), mouse anti-glutathione transferase π (1:500, BD Pharmingen), mouse anti-OCT4 (1:500, Santa Cruz Biotechnology), and the other marker antibodies, hNA, SSEA-1, SSEA-4, TRA-1-60, TRA-1-81, and Nestin (1:100, Chemicon). All secondary antibodies were purchased from Jackson ImmunoResearch. Fluorescent signals were detected by using a confocal laser scanning head (Bio-Rad MRC 1000) on a Zeiss inverted microscope. Images were processed with PHOTOSHOP 7 (Adobe Systems, San Jose, CA).

Laser Capture. Forty-micrometer microtome sections were immunostained with anti-EGFP antibody (1:500, Chemicon), rapidly

Conflict of interest statement: No conflicts declared.

Abbreviations: hESC, human ES cells; EGFP, enhanced GFP; hNA, human nuclear antigen; SSEA, stage-specific embryonic antigen; TBP, TATA-binding protein.

†A.R.M. and K.N. contributed equally to this work.

§To whom correspondence should be addressed. E-mail: gage@salk.edu.

www.pnas.org/cgi/doi/10.1073/pnas.0509315102

Journal of Neurochemistry, 2005, **93**, 432–439 doi:10.1111/j.1471-4159.2005.03031.x

Stage- and site-specific DNA demethylation during neural cell development from embryonic stem cells

Koji Shimozaki,*,‡ Masakazu Namihira,†,‡ Kinichi Nakashima†,‡ and Tetsuya Taga‡

**Laboratory of Animal Molecular Technology, Research and Education Center for Genetic Information, Nara Institute of Science and Technology, Ikoma, Nara, Japan*

†Laboratory of Molecular Neuroscience, Graduate School of Biological Sciences, Nara Institute of Science and Technology, Ikoma, Nara, Japan

‡Department of Cell Fate Modulation, Institute of Molecular Embryology and Genetics, Kumamoto University, Kumamoto, Japan

Abstract

Activation of the transcription factor STAT3 is important for astrocyte differentiation during neural development. Demethylation of the methyl-CpG dinucleotide in the STAT3 binding site in the promoter of the glial fibrillary acidic protein (GFAP) gene, a marker for astrocytes, was previously shown to be a crucial cue for neural progenitors to express this gene in response to astrogenic signals during brain development. In this study, we analyzed the methylation status of the STAT3 binding site in the GFAP gene promoter during neural cell development from mouse embryonic stem (ES) cells *in vitro*. The CpG dinucleotide in the STAT3 binding site in the GFAP gene promoter exhibited a high incidence of cytidine-methylation in undifferentiated pluripotent ES cells. The high incidence of methylation of this particular cytidine was maintained in ES cell-derived neuroectoderm-like cells, but it underwent demethylation when the neural lineage cells became competent to express GFAP in response to a STAT3 activation signal. In contrast, hypermethylation of the CpG site was maintained in non-neural cells generated from the same ES cells. Progressive demethylation of the STAT3 binding site in the GFAP gene promoter was also observed in primary embryonic neuroepithelial cells during *in vitro* culture, whereas non-neural cells maintained hypermethylation of this site even after culture. Taken together, these results demonstrate that the astrocyte gene-specific cytidine-demethylation is programmed when neural progenitors from pluripotent cells are committed to a neural lineage that is capable of producing astrocytes.

Keywords: astrocyte, DNA methylation, embryonic stem cells, glial fibrillary acidic protein, STAT3.

J. Neurochem. (2005) **93**, 432–439.

Epigenetic modification of chromosomal DNA plays multiple important roles in the regulation of cell type-specific gene expression during embryogenesis (Bird and Wolffe 1999). Although neural stem cells mainly differentiate into neurons in the early developing brain, they also become able to produce astrocytes in accordance with the progression of development (Qian *et al.* 2000). Chromosomal DNA in the neural progenitors undergoes epigenetic modification during this change in preference of differentiation (Teter *et al.* 1996; Takizawa *et al.* 2001). We and others have confirmed the importance of the gp130-STAT3 signaling pathway in the development of glial fibrillary acidic protein (GFAP)-expressing astrocytes (Bonni *et al.* 1997; Rajan and McKay 1998; Nakashima *et al.* 1999a,c). We have shown that the cytidine in the CpG dinucleotide in a particular STAT3 recognition element is methylated in neurons and neural progenitors at an early developmental stage (E11.5) when astrogenesis does not normally occur, but demethylated in astrocytes and late-stage (E14.5) neural progenitors that are prone to differentiating into astrocytes (Takizawa *et al.* 2001). We have also demonstrated that demethylation of this CpG site is essential for the development of GFAP-positive astrocytes in response to the STAT3 activation signal

Received September 22, 2004; revised manuscript received December 3, 2004; accepted December 13, 2004.

Address correspondence and reprint requests to Tetsuya Taga, PhD, Department of Cell Fate Modulation, Institute of Molecular Embryology and Genetics, Kumamoto University, 2-2-1, Honjo, Kumamoto, 860–0811, Japan. E-mail: taga@kaiju.medic.kumamoto-u.ac.jp

Abbreviations used: EB, embryoid body; ES, embryonic stem; GFAP, glial fibrillary acidic protein; LIF, leukemia inhibitory factor; MAP2, microtubule-associated protein 2; NS, neural spheroid.

